PIM kinase control of CD8 T cell protein synthesis and cell trafficking

Julia M Marchingo[1,3,#], Laura Spinelli[1,2], Shalini Pathak[1,4], Doreen A Cantrell[1,#]

Affiliations:

1. Cell Signalling and Immunology Division, School of Life Sciences, University of Dundee, United Kingdom
2. Molecular Cell and Developmental Biology Division, School of Life Sciences, University of Dundee, United Kingdom
3. Current address: Blood Cells and Blood Cancer Division, Walter and Eliza Hall Institute of Medical Research, Melbourne, Australia
4. Current address: Innovation Factory Core Technology Facility, University of Manchester, UK

Correspondence: d.a.cantrell@dundee.ac.uk (D.A.C.), marchingo@wehi.edu.au (J.M.M.)

Abstract:

Integration of a large network of kinase signalling pathways co-ordinates changes in the transcription, translation and metabolic events required for T cell activation and differentiation. The present study explores the role of the Serine/Threonine kinases PIM1 and PIM2 in controlling murine CD8 T lymphocyte antigen receptor-mediated activation and differentiation in response to the cytokines Interleukin 2 (IL-2) or IL-15. We show that PIM kinases are dispensable for the differentiation programs controlled by the antigen-receptor and IL-15. There is however a selective role for the PIM kinases in the context of IL-2 regulation of CD8 T cell fate. One key insight was that the PIM kinases controlled the migratory capabilities of effector CD8 T cells, with *Pim1*/*Pim2*-deficient CD8 T cells unable to fully switch off the naïve T cell chemokine and adhesion receptor program during effector differentiation. PIM kinases were also needed for IL-2 to sustain high expression of the glucose transporters SLC2A1 and SLC2A3 and to maintain activity of the nutrient sensing kinase mTORc1. Strikingly, PIM kinases did not have a dominant impact on IL-2-driven transcriptional programs but rather selectively modulated protein synthesis to shape cytotoxic T cell proteomes. This study reveals a selective role of PIM kinases in IL-2 control of CD8 T cells and highlights how regulated changes in protein synthesis can impact T cell phenotypes.

36 **Introduction:**

37 CD8 T lymphocytes are key effector cells for adaptive immune responses to viruses,
38 intracellular pathogens and tumours. Their clonal expansion and differentiation to cytotoxic
39 effector or memory CD8 T cells is controlled by signalling pathways initiated by the T cell
40 antigen receptor (TCR), co-stimulatory molecules and cytokines. Receptor engagement by
41 immune stimuli triggers the activation of cytosolic tyrosine kinases that then direct the
42 activity of a diverse network of Serine/Threonine kinases, disseminating signals from plasma
43 membrane to cell interior. The Src family and ZAP70 Tyrosine kinases initiate this process
44 downstream of the TCR, with the Janus kinases (JAK) as the main signal transducer for
45 important cytokine regulators of T cell differentiation, IL-2 and IL-15 (Cantrell, 2015; Saravia
46 et al., 2020). The subsequent network of Serine/Threonine kinases that is engaged beyond
47 these initiating events coordinates phosphorylation of a diverse array of protein targets.
48 These protein targets include chromatin regulators, transcription factors, translation
49 machinery, cytoskeletal proteins and metabolic enzymes, which then control the changes in
50 transcriptional, translational and metabolic programs that drive effector and memory T cell
51 differentiation (Navarro et al., 2011; Tan et al., 2017; Locard-Paulet et al., 2020).
52
53 CD8 T cells express ∼200 Serine/Threonine protein kinases (Navarro et al., 2014; Howden et
54 al., 2019). There is a good understanding of the roles of some Serine/Threonine kinases in
55 CD8 T cells including the role of the diacylglycerol regulated kinases, MAP kinases ERK1 and
56 2, Phosphatidylinositol (3,4,5) triphosphate- controlled kinases PDK1 and AKT, and the
57 nutrient sensing kinases mammalian Target of Rapamycin complex 1 (mTORc1) and AMP-
58 activated protein kinase (AMPK) (Finlay et al., 2012; Rolf et al., 2013; Blagih et al., 2015;
59 Cantrell, 2015; Hukelmann et al., 2016; Tan et al., 2017; Howden et al., 2019; Saravia et al.,
60 2020; Damasio et al., 2021; Spinelli et al., 2021). However, beyond these core kinases there
61 is much still to learn about how many of the ~200 Serine/Threonine kinases expressed in
62 CD8 T cells contribute to the control of T cell function. In this context, the PIM kinases are a
63 family of Serine/Threonine kinases that are strongly and rapidly induced in T cells
64 responding to immune stimuli (Aho et al., 2005; Fox et al., 2005; Peperzak et al., 2010;
65 Jackson et al., 2012). The PIM family contains 3 Serine/Threonine kinases, PIM1, PIM2 and
66 PIM3, of which T lymphocytes predominantly express PIM1 and PIM2 (Mikkers et al., 2004;
67 Fox et al., 2005). As PIM kinases are constitutively active, their participation in signalling

68 cascades is dictated by regulated changes in their protein expression levels (Warfel and
69 Kraft, 2015). PIM1 and PIM2 have little to no expression in naïve T cells but are induced by
70 T-cell receptor activation and costimulation (e.g. CD27) (Wingett et al., 1996; Fox et al.,
71 2005; Peperzak et al., 2010). PIM kinases are also direct transcriptional targets of JAK/STAT
72 signalling pathways and as such PIM1 and/or PIM2 are rapidly induced in T cells
73 downstream of a diverse array of cytokines, including multiple common cytokine receptor γ-
74 chain family cytokines, IL-6 and IL-12 (Matikainen et al., 1999; Aho et al., 2005; Fox et al.,
75 2005; Warfel and Kraft, 2015; Buchacher et al., 2023).
76
77 There have been some analyses of how deletion of PIM kinases impacts CD8 T cell function.
78 A mild reduction in *Pim1/Pim2/Pim3*-deficient CD4 and CD8 T cell proliferation has been
79 observed in response to sub-optimal TCR stimulation and IL-2 (Mikkers et al., 2004) and
80 there is evidence that PIM1 and PIM2 control survival pathways in naïve CD4 and CD8 T cells
81 in concert with mTORc1 (Fox et al., 2005). *Pim1/Pim2/Pim3* deletion is reported to promote
82 expression of stemness and memory-associated transcription factors including Bcl6 and Tcf7
83 (Chatterjee et al., 2019) and PIM kinase activity has been linked with maintenance of
84 memory CD8 T cell survival (Knudson et al., 2017). It has also been shown recently that
85 *Pim1/Pim2* deficiency prevented mTORc1 activation and the proliferation of non-
86 conventional intra-epithelial gut CD8 T lymphocytes (IEL) in response to the cytokine IL-15
87 (James et al., 2021).
88
89 Elevated PIM kinase expression has been noted in patient T cells for a number of
90 autoimmune conditions, including rheumatoid arthritis, uveitis and coeliac disease, and PIM
91 kinase inhibition has been proposed as a possible intervention to dampen autoimmunity
92 (James et al., 2021; Maney et al., 2021; Li et al., 2022). PIM kinase inhibitors have also
93 entered clinical trials to treat some cancers and there is active interest in combining these
94 with immunotherapies (Clements and Warfel, 2022). Given the role of CD8 T cells in anti-
95 cancer immunity, it is important to understand how these kinase control CD8 T cell function.
96 However, there has not yet been a systematic analysis of the role of PIM kinases in
97 conventional CD8 T cells as they activate and differentiate to form effector and memory
98 cells. Accordingly, the current study, uses high resolution quantitative analysis of
99 *Pim1*/*Pim2*-deficient CD8 T cell proteomes and transcriptomes to obtain a comprehensive

100 and unbiased understanding of how PIM kinases control CD8 T cell TCR-driven activation,
101 and IL-2 or IL-15-driven proliferation, and differentiation. The study reveals a selective role
102 for PIM kinases as mediators of IL-2 signalling to control CD8 T cell trafficking and effector
103 functionality. We uncover that the dominant impact of PIM kinase loss was to shape
104 effector CD8 T cell proteomes rather than transcriptomes, reflecting PIM kinase modulation
105 of protein synthesis.
106
107 **Results:**
108 ***PIM1 and PIM2 are strongly induced by antigen receptor engagement but are dispensable***
109 ***for T cell activation***
110 T cell antigen receptor (TCR) -driven activation of naïve T cells initiates their clonal
111 expansion and differentiation into effector and memory cells. Quantitative mass
112 spectrometry-based proteomics analysis of naïve OT1 CD8 T cell stimulated with their
113 cognate peptide over time (Marchingo et al., 2020) showed that PIM1 protein was strongly
114 induced within 3 hours of TCR engagement, which was sustained at a 24 hour time point
115 (**Fig 1A**). PIM2 expression was not detected until 9 hours post-stimulation but was also
116 sustained at the 24 hour time point. 24 hour polyclonal activation of CD8 T cells with
117 αCD3/αCD28 agonist antibodies similarly induced expression of PIM1 and PIM2 proteins
118 (**Fig 1B, Table S1**). These increases in PIM kinases expression at a protein level were
119 underpinned by transcriptional reprograming, with both *Pim1* and P*im2* mRNA very lowly
120 expressed in naïve CD8 T cells and strongly upregulated by immune activation (**Fig 1C**)
121 (Spinelli et al., 2021). Consistent with previous reports of Pim1 and Pim2 being the major
122 PIM kinases in T cells (Mikkers et al., 2004; Fox et al., 2005), *Pim3* mRNA was only expressed
123 at very low levels in naïve and activated CD8 T cells (**Fig 1C**), with PIM3 protein not detected
124 at all by mass spectrometry (**Table S1**).
125
126 PIM1 and PIM2 have similar substrate selectivity and hence functional redundancy (Mikkers
127 et al., 2004; Bullock et al., 2005; Fox et al., 2005; Peng et al., 2007; Warfel and Kraft, 2015).
128 Accordingly, to explore the role of the PIM kinases in T cells, mice with a whole body
129 deletion of *Pim1* and *Pim2*, Pim1$^{-/-}$ (Pim1 KO) (Laird et al., 1993) and Pim2$^{-/-}$ or Pim2$^{-/Y}$ (Pim2
130 KO) (Mikkers et al., 2004), were backcrossed for >10 generations onto a C57BL/6
131 background and inter-crossed to generate *Pim1*/*Pim2* double knockout (Pim dKO) mice.

132 There were normal proportions of peripheral T cells in spleens of Pim dKO mice, though the
133 total number of splenocytes was lower than in age/sex matched wild-type (WT) mice (**Fig**
134 **S1A-C**). However, Pim dKO T cells showed a normal increase in cell size in response to
135 immune activation with αCD3/αCD28 agonist antibodies (**Fig 1D**) and 24 hour αCD3/αCD28
136 activated Pim dKO CD4 and CD8 T cells exhibited normal upregulation of established
137 markers of T cell activation including CD25, CD44 and the transferrin receptor CD71 (**Fig 1E**).
138 24 hour TCR-activated Pim dKO CD8 T cells also produced normal levels of the key effector
139 cytokine IFNγ (**Fig 1E**) and there was no discernible difference in TCR-driven proliferation
140 between WT and Pim dKO T cells over 3 days in culture (**Fig 1F, J**). To systematically explore
141 in an unbiased way if *Pim1*/*Pim2*-deficiency impacted TCR-driven activation phenotypes, we
142 performed high-resolution mass spectrometry to measure the proteomes of 24 hour
143 αCD3/αCD28 activated WT and Pim dKO CD4 and CD8 T cells. These experiments quantified
144 expression of >7000 proteins but found no substantial quantitative or qualitative differences
145 in protein content or proteome composition in activated WT versus Pim dKO CD4 and CD8 T
146 cells (**Fig 1G-H**) (**Table S1**), indicating a redundancy between PIM kinases and other
147 signalling pathways downstream of TCR activation.
148
149 One prominent study has reported that *Pim1*/*Pim2* deficiency sensitises T cells to the
150 mTORc1 inhibitor rapamycin (Fox et al., 2005), which suggests mTORc1 as a candidate for
151 mediating this redundancy. This study showed naïve Pim dKO T cells cultured in IL-7 died in
152 response to rapamycin treatment, whereas WT cells did not, and that rapamycin synergised
153 with *Pim1*/*Pim2*-deficiency to substantially reduce TCR-driven activation and proliferation
154 (Fox et al., 2005). However, we found no impact of *Pim1*/*Pim2*-deficiency on the ability of
155 naïve CD8 T cells cultured with IL-7 to survive in response to rapamycin treatment (**Fig 1I**).
156 Furthermore, we found no difference in the effect of rapamycin on mean division number in
157 Pim dKO versus WT CD8 T cells (**Fig 1J**). Collectively these data show that PIM 1 and PIM2
158 are rapidly and strongly expressed in response to immune activation, but they are
159 dispensable for the antigen receptor-driven proteome remodeling that initiates T cell clonal
160 expansion and differentiation. We also found no evidence that the *Pim1* and *Pim2* loss
161 synergised with mTORC1 inhibition.
162
163

164 ***PIM kinases do not control IL-15-driven CD8 T cell memory differentiation***

165 The proliferative expansion and differentiation programs of CD8 T cells are shaped by
166 cytokines. In this context, PIM1 and PIM2 kinase expression is regulated by the cytokines IL-
167 2 and IL-15 which are key to shaping CD8 T cell effector and memory cell differentiation
168 respectively (Weninger et al., 2001; Cornish et al., 2006; Buck et al., 2016). Both IL-2 and IL-
169 15 control PIM1 and PIM2 expression in antigen primed CD8 T cells (**Fig 2A**). Accordingly, we
170 assessed the contribution of PIM1 and PIM2 kinases to cytokine-driven expansion and
171 differentiation of antigen activated CD8 T cells. In these experiments, antigen-primed CD8 T
172 cells are expanded in IL-15 to generate memory phenotype CD8 T cells or expanded in IL-2
173 to generate effector cytotoxic T lymphocytes (CTL) (Weninger et al., 2001; Cornish et al.,
174 2006; Buck et al., 2016) (**Fig 2B**).

175

176 Previous work has shown that PIM1 and PIM2 mediate IL-15 induced proliferation of gut
177 intra-epithelial lymphocytes (IEL) (James et al., 2021). However, their role in IL-15 responses
178 in conventional antigen receptor activated CD8 T cells is not known. We therefore first
179 examined the impact of *Pim1/Pim2*-deficiency on IL-15-driven conventional CD8 T cell
180 expansion. Antigen experienced WT CD8 T cells show a robust proliferative response to IL-
181 15 such that there is an ~90-fold expansion of the CD8 T cells between days 2 and 6 of
182 culture (**Fig 2C**). There was no impact of *Pim1*/*Pim2*-deficiency on the ability of IL-15 to
183 sustain CD8 T cell viability (**Fig 2D**). Immune activated Pim dKO CD8 T cells also proliferated
184 strongly in response to IL-15, but showed a moderate proliferative disadvantage resulting in
185 a ~4-fold difference in total cell number by day 6 of the culture (**Fig 2C**). Antigen-primed CD8
186 T cells expand in IL-15 to generate memory phenotype CD8 T cells (Weninger et al., 2001).
187 We therefore examined whether *Pim1*/*Pim2*-deficiency had any impact on the ability of IL-
188 15 to induce memory differentiation. Accordingly, we performed parallel bulk RNAseq and
189 high-resolution mass spectrometry to analyse the transcriptome and proteome of IL-15
190 expanded WT and Pim dKO CD8 T cells. The RNAseq analysis quantified ~14,000 RNA and
191 using a cut off of >1.5 fold-change and q-value <0.05 we saw that the abundance of 381 RNA
192 was modified by *Pim1*/*Pim2*-deficiency (**Fig 2E**) (**Table S2A**). Of the 381 RNA that were
193 detected as differentially expressed (FC>1.5, q<0.05) only ~30% were detected with an
194 average expression over 10 transcripts per million (TPM), of these gene ~36% were non-
195 coding RNA, uncharacterised genes or pseudogenes, leaving only 72 substantially expressed

196 protein coding mRNA that were differentially expressed in Pim dKO versus WT IL-15
197 expanded CD8 T cells (**Table S2B**). These data indicate that Pim1/Pim2-deficiency has very
198 little effect on IL-15 induced protein-coding mRNA expression in differentiated T cells. We
199 then specifically examined if Pim dKO T cells had any differences in mRNA that are known to
200 be critical for memory cell differentiation. We found that *Pim1*/*Pim2*-deficiency did not
201 decrease expression of mRNA levels for critical memory T cell genes such as the adhesion
202 molecules and chemokine receptors, *Sell* (CD62L), *Ccr7* and *S1pr1* that direct the trafficking
203 of CD8 T cells to secondary lymphoid tissue. (**Fig 2F**). *Pim1/Pim2*-deficiency also did not
204 reduce expression of mRNA for the key memory cell transcription factors *Tcf7, Foxo1, Foxo3*
205 *Klf2 and Id3.* (**Fig 2G**). Indeed, if anything, there were small increases in expression of the
206 *Klf2*, *Id3* and *Ccr7* mRNA in Pim dKO versus WT IL-15 expanded CD8 T cells (**Fig 2F-G**).
207 Critically, when the proteomes of IL15 expanded WT and Pim dKO CD8 T cells were analysed
208 and expression of ~6900 total proteins quantified, there were no major changes in the
209 proteomes between WT and Pim dKO IL15 expanded CD8 T cells (**Fig 2H, Table S3**). Of note,
210 the mitochondrial proteome composition of IL15 expanded WT and Pim dKO CD8 T cells
211 were indistinguishable (**Fig 2I-J**). This is pertinent because one key feature of how IL-15
212 controls memory T cells is via mitochondrial remodelling to support energy production via
213 oxidative phosphorylation and fatty acid oxidation (Buck et al., 2016) and it has been
214 described that PIM kinases can control mitochondrial phenotypes in cancer cell lines and
215 cardiomyocytes (Din et al., 2013; Chauhan et al., 2020). These data show that PIM1 and
216 PIM2 do not drive IL-15-mediated metabolic or differentiation programs in antigen-primed
217 CD8 T cells.
218
219 ***PIM kinases selectively modulate IL-2 controlled effector CD8 T cell differentiation***
220 IL-2 controls the expression of PIM1 and PIM2 kinases (**Fig 2A**) and in this context, we noted
221 that the copy numbers per cell of PIM1 protein is considerably higher in actively expanding
222 antigen-activated CD8 cells maintained with IL-2 compared to IL-15 (**Fig 3A**)**.** We therefore
223 examined the role of PIM1 and PIM2 in the IL-2 signalling pathways that control the
224 differentiation of effector CTL. The data show that Pim dKO antigen activated CD8 T cells
225 responded normally to IL-2 to induce STAT5 Y694 phosphorylation (**Fig 3B**). They also
226 express normal levels of the IL-2-receptor alpha chain, CD25, (**Fig 3C**), which is sustained by
227 STAT5, and together these data broadly indicate IL-2 receptor signal transduction is

228 unaltered by *Pim1*/*Pim2*-deficiency. Antigen activated WT CD8 T cells have a strong survival
229 and proliferative response to IL-2 producing an ~270-fold expansion between days 2 and 6
230 of culture in saturating IL-2 concentrations (**Fig 3D**). There was no impact of *Pim1*/*Pim2*-
231 deficiency on the ability of IL-2 to maintain CD8 T cell viability (**Fig 3E**) and Pim dKO cells CD8
232 T cells cultured in IL-2 proliferated robustly. They did however exhibit a very mild
233 proliferative disadvantage resulting in a ~2-fold difference in total cell number by day 6 of
234 the culture (**Fig 3D).** We then examined whether *Pim1*/*Pim2*-deficiency had any impact on
235 the differentiation of Pim dKO CD8 T cells into effector CTL. Expression of activation markers
236 CD44 and CD71 in IL-2-expanded CTL were similar between WT and Pim dKO CD8 T cells on
237 days 3 and 6 of co-cultures (**Fig 3F**). However, one consistent difference between IL-2
238 maintained WT and Pim dKO CD8 T cells is that WT CTL downregulated expression of CD62L
239 (L-selectin, *Sell*), whereas the Pim dKO CTL sustained higher CD62L expression (**Fig 3G**). We
240 also noted that IL-2 maintained Pim dKO CTL had reduced forward and side scatter
241 properties i.e were smaller and less granular than corresponding WT CTL (**Fig 3F).**
242
243 To explore the apparent size change between Pim dKO and WT IL-2 expanded CTL, we used
244 high resolution mass spectrometry to compare the proteomes of day 6 IL-2 cultured WT or
245 Pim dKO CTL. These analyses quantified expression of ~6,900 proteins and showed a small
246 decrease in the total protein mass of IL-2 maintained Pim dKO CD8 T cells compared to WT
247 cells (**Fig 4A, Table S4**). The data showed down-regulation of the expression of 513 proteins
248 (>1.5 fold-change, q<0.05) in Pim dKO CTL along with increased copy numbers of 33 proteins
249 (**Fig 4B**, **Table S4**). The transcription factor profile of Pim dKO T cells was consistent with
250 that of an effector CTL with high levels of TBX21 and low levels of TCF1 (*Tcf7*) (**Fig 4C**). Pim
251 dKO T cells also exhibited an effector-like mitochondrial proteome profile (**Fig S2**). However,
252 there were salient differences in proteins important for effector functionality between WT
253 and Pim dKO CD8 T cells. These included lower levels of the glucose transporters, SLC2A1
254 and SLC2A3 (GLUT1 and GLUT3) (**Fig 4D**) which are the major glucose transporters in CD8 T
255 cells (Hukelmann et al., 2016) and are key for enabling T cells to fuel high rates of glycolysis
256 and protein O-GlcNAcylation required to support effector functions(Chang et al., 2015;
257 Swamy et al., 2016). Pim dKO CTL also had decreased expression of a number of proteins
258 involved in fatty acid and cholesterol biosynthesis including SCD2, HMGCS1, MVK, IDI1,
259 FDPS, FDFT1 and SQLE (**Fig 4E**). Another striking observation was that the Pim dKO CD8 cells

260 had reduced levels of a number of key effector proteins including multiple granzymes,
261 perforin, IFNγ and TNFα (**Fig 4F**). Orthogonal flow cytometric analysis of Granzyme B and
262 IFNγ levels confirmed reduced levels of these effector molecule in IL-2 expanded Pim dKO
263 CTL, though IFNγ protein is only lowly produced in IL2 maintained CTL. (**Fig 4G).** In parallel
264 experiments we also examined the impact of an acute loss of PIM kinase activity on the
265 proteomes of IL-2 maintained CTL to see if this could recapitulate key observations from Pim
266 dKO T cells. When IL-2 maintained WT CTL were treated for 24 hours with the pan-PIM
267 kinases inhibitors PIM447 or AZD1208 we saw reductions in cell proliferation, cell size, cell
268 granularity, fatty acid biosynthesis proteins SCD1-3, glucose transporters SLC2A1, SLC2A3
269 and a reduction in Granzyme B expression (**Fig S3A-E, Table S5**). This corroborated some key
270 observations from the experiments with Pim dKO CTL, where *Pim1* and *Pim2* had been
271 deleted over the lifespan of the T cell.
272
273 To examine the molecular regulation underpinning PIM1 and PIM2 kinase control of key
274 metabolic and effector proteins we also performed RNAseq on IL-2 differentiated WT and
275 Pim dKO CTL samples collected in parallel with the proteomics analysis described in Fig 4. In
276 these experiments ~14,000 mRNA were quantified and using a cut off >1.5 fold-change,
277 q<0.05 we saw that the abundance of 223 mRNA were decreased and 155 increased by
278 *Pim1*/*Pim2* deficiency (**Fig 5A, Table S6**). These data revealed that the reduced expression of
279 perforin and Granzymes C-G and K protein corresponded to decreases in their mRNA (**Fig**
280 **5B-C**). However, there were striking examples where a clear decrease in protein levels did
281 not correspond with an appreciable decrease in mRNA expression. These included the
282 predominant cytolytic Granzymes B and A (**Fig 5C-D**), as well as both glucose transporters
283 SLC2A1 and SLC2A3 (**Fig 5E**). Furthermore, contrasting differential expression of proteins
284 and mRNA data in Pim dKO vs WT CTL revealed that ~75 % of the proteins whose expression
285 was changed in Pim dKO T cells (FC>1.5, q<0.05), exhibited no strong corresponding changes
286 in their mRNA (FC<1.2) (**Fig 5F, Table S7**). Indeed, of the ~500 proteins whose expression
287 decreased at the protein level in Pim dKO CTL only 17 showed a strong decrease in
288 magnitude at the mRNA level as well (**Fig 5G, Table S7**).
289 These observations could reflect that the PIM kinases are required for IL-2 to maximally
290 control protein synthesis in CD8 T cells. To examine this hypothesis we first interrogated our
291 proteomics and transcriptomics data. Consistent with this hypothesis we observed a small

292 reduction in ribosome protein content in Pim dKO CTL, which scaled with the reduction in
293 total protein content (**Fig 5H**). Moreover the translational repressor PDCD4 was increased in
294 Pim dKO CTL (**Fig 5I**). This could be confirmed by flow cytometry (**Fig 5J**) and was
295 underpinned at the mRNA level (**Fig 5B**). Similarly, 24 hour inhibition with pan PIM kinases
296 inhibitors was sufficient to substantially increase PDCD4 protein expression (**Fig S3F**). We
297 also noted that there was a small decrease in the expression of EIF4A1, a key component of
298 the eIF4F translation initiation complex, in Pim dKO IL2 maintained CTL (**Fig 5K**). PDCD4
299 inhibits translation by binding EIF4A1 in a 2:1 ratio, preventing its interaction with the EIF4F
300 complex (Suzuki et al., 2008). Together the changes in both proteins equated to an
301 approximate halving of the ratio between EIF4A1 and PDCD4 (**Fig 5L**). These data all support
302 that loss of PIM kinases could reduce protein synthesis in IL-2 maintained CTL. To test this
303 hypothesis we used a single cell assay that quantifies the incorporation of an analogue of
304 puromycin (OPP) into newly synthesized protein chains in the ribosome to assess cellular
305 rates of protein synthesis. We found that 24 hours of treatment with pan-PIM kinase
306 inhibitors PIM447 or AZD1208 caused a quantitative reduction in protein synthesis rates of
307 IL-2 expanded CTL (**Fig 5M)**. This data is consistent with PIM kinase effects on protein
308 expression being via control of protein translation.
309
310 ***PIM1 and PIM2 regulate mTORc1 and sustain lymphoid homing in Pim1/Pim2-deficient***
311 ***effector CTL***
312 The pattern of proteome remodelling in Pim dKO CTL had some phenotypic features in
313 common with the previously reported changes that occur following inhibition of the
314 Serine/Threonine kinase mTORc1 in CTL (Hukelmann et al., 2016; Howden et al., 2019).
315 These included: increased expression of PDCD4 and decreased expression of cholesterol
316 biosynthesis enzymes and effector molecules including granzymes, perforin, IFNγ and TNFα
317 (Hukelmann et al., 2016; Howden et al., 2019). In this respect, mTORc1 activity in CTL is
318 acutely sensitive to reduced availability of glucose (Rolf et al., 2013) and the reduced
319 expression of glucose transporters in Pim dKO T cells might predict that these cells would
320 have lower activity of mTORc1. We therefore assessed if PIM kinases were required for IL-2
321 activation of mTORc1. In these experiments we compared the phosphorylation of S6K1 (p70
322 S6-kinase 1) on its mTORC1 substrate sequence T389 in WT and Pim dKO CD8 T cells by
323 western blot. These data show a modest reduction of mTORc1 activity in the Pim dKO T cells

324 (**Fig 6A**). We also assessed the activity of S6K1 at a single cell level by quantifying the
325 phosphorylation of its downstream target protein S6 ribosomal protein on S235/S236 by
326 flow cytometry over the course of IL-2 driven CTL expansion. These data also show that
327 *Pim1/Pim2*-deficiency reduced IL-2 induced mTORc1 dependent phosphorylation of S6 but
328 did not compromise the ability of the Pim dKO cells to phosphorylate S6 in response to
329 phorbol esters and calcium ionophores; pharmacological activators that induce RSK
330 mediated S6 phosphorylation (**Fig 6B**).
331
332 Previously, it has been shown that decreased glucose availability or inhibition of mTORc1
333 prevents the downregulation of CD62L that normally accompanies IL-2 induced CTL
334 differentiation (Sinclair et al., 2008; Finlay et al., 2012). Thus, the reduced expression of
335 glucose transporters and reduced activity of mTORc1 in Pim dKO IL-2 expanded CTL provides
336 a potential explanation for the striking phenotype shown in Fig 3G, that IL-2 maintained Pim
337 dKO CTL retain high levels of CD62L/L-selectin. The IL-2 CTL transcriptomics data showed
338 there is increased expression of CD62L at the mRNA level in IL-2 maintained PimdKO CTL (**Fig**
339 **5B, 6C**). The expression of *Sell* (CD62L) mRNA is controlled by the transcription factor KLF2
340 and the expression of *Klf2* mRNA is also increased in IL-2 maintained Pim dKO CTL (**Fig 6D**) as
341 are mRNA levels for other KLF2 targets: the chemokine receptors *Ccr7* and *S1pr1 (***Fig 6C***)*.
342
343 CD62L/L-selectin controls T cell adhesion to the endothelium of high endothelial venules
344 and is essential for lymphocyte transit from blood into secondary lymphoid tissue such as
345 lymph nodes. CCR7, and the $S1P_1$ receptor also direct migration by controlling T cell entry
346 and egress respectively into secondary lymphoid tissue. In this context, the loss of CD62L,
347 CCR7 and S1PR1 expression following immune activation reprograms the trafficking of
348 effector T cells away from lymphoid tissue toward sites of inflammation in peripheral tissues
349 (Sinclair et al., 2008; Nolz et al., 2011). Accordingly, the differences between Pim dKO and
350 WT CTL in terms of CD62L expression could indicate that in addition to having reduced
351 effector protein expression, Pim dKO CTL also do not switch their trafficking behaviour to
352 that of a fully differentiated effector CTL and rather retain the capacity to home to lymphoid
353 tissues. To test this possibility *in vivo*, we performed adoptive transfer experiments
354 comparing the ability of WT effector CTL and Pim dKO CTL to home to secondary lymphoid

355 tissues. In these experiments, αCD3/αCD28 activated WT or Pim dKO T cells were
356 differentiated in IL-2 and cells then were labelled with either CFSE or CTV dyes; mixed at a
357 ratio of 1:1, and adoptively transferred into C57BL/6 hosts. **Fig 6E** shows that Pim dKO CTL,
358 but not WT CTL, retained substantial capacity to home to secondary lymphoid organs and,
359 hence, accumulated in lymph nodes and spleen: PIM kinases are thus required for the
360 normal reprogramming of CTL trafficking.
361
362 **Discussion:**
363 The objective of the present study was to use quantitative analysis of T cell proteomes and
364 transcriptomes to explore how deletion of the Serine/Threonine kinases PIM1 and PIM2
365 impacts CD8 T cell activation and differentiation. The expression of PIM1 and PIM2 is
366 induced during immune activation of CD8 T cells by antigen and co-stimulation and then
367 sustained to varying degrees by the cytokines IL2 or IL-15. The loss of PIM1 and PIM2 was
368 shown to have no effect on the CD8 T cell programs controlled by antigen receptor/co-
369 stimulation and had very little impact on the IL-15-driven transcriptional and proteomic
370 programs in memory differentiated CD8 T cells. However, PIM1 and PIM2 were required for
371 IL-2 programming of effector CD8 T cell differentiation. IL-2 controls essential cytolytic
372 effector and metabolic programs in CTL, is a key cytokine for CD8 T cell anti-viral immunity
373 and is also used to produce cytotoxic T cells for anti-cancer immunotherapy (Kalia and
374 Sarkar, 2018). The understanding that PIM kinases mediate IL-2 control of the expression of
375 glucose transporters, lipid metabolic enzymes and key cytolytic proteins such as granzymes
376 A and B in effector CD8 T cells is thus fundamental information about how this key cytokine
377 controls T cells. It was also important to understand that PIM kinases did not control the
378 transcriptional programs that direct expression of glucose transporters and effector
379 enzymes and the hence the full consequences of PIM kinase deletion could only be assessed
380 by in depth analysis of the proteomes of *Pim1*/*Pim2*-deficient CTL and not from mRNA
381 sequencing. The loss of PIM kinase activity reduced protein synthesis rates in CTL which
382 explains the discordance between mRNA and protein reported herein. The reduction in
383 protein synthesis was modest but previous studies have shown that modest reductions in
384 protein synthesis and loss of mTORc1 activity impact CD8 T cell differentiation programs
385 (Cornish et al., 2006; Hukelmann et al., 2016; Howden et al., 2019). PIM kinase regulation of
386 protein translation has been reported previously in mouse B cell lymphoma and mouse

387 embryonic fibroblasts (Schatz et al., 2011) and some of the key examples of proteins we
388 found to be unaltered at the mRNA level but down-regulated at the protein level have prior
389 reports of sensitivity to translational regulation in immune cells (Fehniger et al., 2007;
390 Ricciardi et al., 2018). Reduced protein synthesis capacity in cells lacking PIM kinases could
391 be caused by reduced mTORc1 activity combined with increased expression at the mRNA
392 and protein level of the translational repressor PDCD4. Moreover, protein synthesis is highly
393 energetically demanding and once CTL have reduced glucose transporter expression this
394 would reduce glucose availability to fuel protein production. These data collectively point
395 towards modulation of protein translation as an important target of PIM kinase activity
396 downstream of IL-2 in CD8 T cells.
397
398 One other important insight from the current work is that PIM kinases are required for IL2
399 to fully repress expression of the adhesion molecule CD62L and the chemokine receptors
400 CCR7 and S1PR1. These molecules play a key role in controlling T cell homing to secondary
401 lymphoid tissue and are expressed at high levels in naïve and memory T cells. IL-2 induces
402 down regulation of CD62L, CCR7 and S1PR1 expression as part of a program that causes
403 effector cells to lose their capacity to home to secondary lymphoid tissues (Sinclair et al.,
404 2008; Nolz et al., 2011). The present data show that PIM kinases can mediate this IL-2
405 repression of lymph node homing receptors and the ability of IL-2 to switch off the naïve T
406 cell trafficking program. IL2 maintained Pim dKO CD8 effector T cells thus retain the capacity
407 to home to secondary lymphoid tissues *in vivo*. This lymph-node homing pattern is also a
408 memory CD8 T cell phenotype but here it is pertinent that the current in-depth analysis of
409 the transcriptomes and proteomes of *Pim1*/*Pim2*-deficient IL-2 differentiated CD8 T cells
410 show that the loss of PIM kinases does not cause effector T cells to differentiate instead into
411 memory cells. For example, IL-2 maintained Pim dKO CD8 T cells do not re-express key
412 molecules that maintain the stem-like properties of memory cells such as the transcription
413 factor TCF7 and IL-7 receptor (Table S2, S6). Nor do Pim dKO CTL cultured in IL-2 have the
414 mitochondrial proteome of a memory T cell. Hence *Pim1*/*Pim2*-deficiency prevents optimal
415 differentiation of effector CTL but does not cause these cells to fully switch to a memory
416 phenotype. This is worth knowing as pan-PIM kinase inhibitors are in development as anti-
417 cancer drugs and it has been suggested that PIM inhibitors might be used as a strategy to
418 generate more stem-memory-like CD8 T cells in combination with cancer immunotherapy

419 treatments (Chatterjee et al., 2019; Clements and Warfel, 2022). Information about how the
420 loss of PIM kinases will impact CD8 T cells is very relevant to informed usage of such drugs.
421
422 Finally, the selectivity of PIM kinases for IL-2 control of conventional CD8 T cell
423 differentiation with no evidence that PIMs were important for IL-15 responses beyond a
424 modest effect on cell proliferation was interesting. This failure to see a role for PIM
425 signalling in conventional peripheral CD8 T cell differentiation is in contrast to observations
426 that PIM1 and PIM2 direct IL15 control of the metabolic programming of intestinal IEL
427 (James et al., 2021). A notable difference between these scenarios was that in IEL, IL15 was
428 being used individually to drive immune activation and was sufficient to strongly induce
429 PIM1 and PIM2 expression. In contrast, in our conventional CD8 T cell system we uncovered
430 that that IL-15 does not sustain high levels of PIM kinases, which could possibly explain this
431 discrepancy. However, high levels of PIM expression alone are not inevitably predictive of
432 their importance. In this study we observed very high levels of both PIM1 and PIM2 in
433 antigen activated CD8 T cells yet loss of PIM kinases there had no functional impact. There
434 are thus clearly redundant kinase pathways that can substitute for the PIM kinases in the
435 immediate response of CD8 T cells to immune activation. Previously it was suggested that
436 mTORc1 may be one of these pathways (Fox et al., 2005), however we found no evidence
437 for that here, and in fact observed that PIM kinase deficiency was upstream of a reduction
438 in mTORc1 activity in IL2 expanded CTL. Thus, this examination of the role of PIM kinases in
439 multiple signalling situations reveal cell context dependent regulatory roles for PIM kinases
440 rather than hard wired functions that apply to every stimulatory situation in T cells.
441

442 **References:**

443 Aho, T. L., R. J. Lund, E. K. Ylikoski, S. Matikainen, R. Lahesmaa, and P. J. Koskinen. 2005.
444 Expression of human pim family genes is selectively up-regulated by cytokines
445 promoting T helper type 1, but not T helper type 2, cell differentiation. *Immunology*
446 116: 82-88.
447 Blagih, J., F. Coulombe, E. E. Vincent, F. Dupuy, G. Galicia-Vazquez, E. Yurchenko, T. C. Raissi,
448 et al. 2015. The energy sensor AMPK regulates T cell metabolic adaptation and
449 effector responses in vivo. *Immunity* 42: 41-54.
450 Buchacher, T., A. Shetty, S. A. Koskela, J. Smolander, R. Kaukonen, A. G. G. Sousa, S. Junttila,
451 et al. 2023. PIM kinases regulate early human Th17 cell differentiation. *Cell Rep* 42:
452 113469.
453 Buck, M. D., D. O'Sullivan, R. I. Klein Geltink, J. D. Curtis, C. H. Chang, D. E. Sanin, J. Qiu, et al.
454 2016. Mitochondrial Dynamics Controls T Cell Fate through Metabolic Programming.
455 *Cell* 166: 63-76.
456 Bullock, A. N., J. Debreczeni, A. L. Amos, S. Knapp, and B. E. Turk. 2005. Structure and
457 substrate specificity of the Pim-1 kinase. *J Biol Chem* 280: 41675-41682.
458 Cantrell, D. 2015. Signaling in lymphocyte activation. *Cold Spring Harb Perspect Biol* 7.
459 Chang, C. H., J. Qiu, D. O'Sullivan, M. D. Buck, T. Noguchi, J. D. Curtis, Q. Chen, et al. 2015.
460 Metabolic Competition in the Tumor Microenvironment Is a Driver of Cancer
461 Progression. *Cell* 162: 1229-1241.
462 Chatterjee, S., P. Chakraborty, A. Daenthanasanmak, S. Iamsawat, G. Andrejeva, L. A.
463 Luevano, M. Wolf, et al. 2019. Targeting PIM Kinase with PD1 Inhibition Improves
464 Immunotherapeutic Antitumor T-cell Response. *Clin Cancer Res* 25: 1036-1049.
465 Chauhan, S. S., R. K. Toth, C. C. Jensen, A. L. Casillas, D. F. Kashatus, and N. A. Warfel. 2020.
466 PIM kinases alter mitochondrial dynamics and chemosensitivity in lung cancer.
467 *Oncogene* 39: 2597-2611.
468 Clements, A. N., and N. A. Warfel. 2022. Targeting PIM Kinases to Improve the Efficacy of
469 Immunotherapy. *Cells* 11.
470 Cornish, G. H., L. V. Sinclair, and D. A. Cantrell. 2006. Differential regulation of T-cell growth
471 by IL-2 and IL-15. *Blood* 108: 600-608.
472 Damasio, M. P., J. M. Marchingo, L. Spinelli, J. L. Hukelmann, D. A. Cantrell, and A. J. M.
473 Howden. 2021. Extracellular signal-regulated kinase (ERK) pathway control of CD8+ T
474 cell differentiation. *Biochem J* 478: 79-98.
475 Din, S., M. Mason, M. Volkers, B. Johnson, C. T. Cottage, Z. Wang, A. Y. Joyo, et al. 2013. Pim-
476 1 preserves mitochondrial morphology by inhibiting dynamin-related protein 1
477 translocation. *Proc Natl Acad Sci U S A* 110: 5969-5974.
478 Dobin, A., C. A. Davis, F. Schlesinger, J. Drenkow, C. Zaleski, S. Jha, P. Batut, et al. 2013. STAR:
479 ultrafast universal RNA-seq aligner. *Bioinformatics* 29: 15-21.
480 Ewels, P., M. Magnusson, S. Lundin, and M. Kaller. 2016. MultiQC: summarize analysis results
481 for multiple tools and samples in a single report. *Bioinformatics* 32: 3047-3048.
482 Fehniger, T. A., S. F. Cai, X. Cao, A. J. Bredemeyer, R. M. Presti, A. R. French, and T. J. Ley.
483 2007. Acquisition of murine NK cell cytotoxicity requires the translation of a pre-
484 existing pool of granzyme B and perforin mRNAs. *Immunity* 26: 798-811.
485 Finlay, D. K., E. Rosenzweig, L. V. Sinclair, C. Feijoo-Carnero, J. L. Hukelmann, J. Rolf, A. A.
486 Panteleyev, et al. 2012. PDK1 regulation of mTOR and hypoxia-inducible factor 1
487 integrate metabolism and migration of CD8+ T cells. *J Exp Med* 209: 2441-2453.

488 Fox, C. J., P. S. Hammerman, and C. B. Thompson. 2005. The Pim kinases control rapamycin-
489 resistant T cell survival and activation. *J Exp Med* 201: 259-266.
490 Howden, A. J. M., J. L. Hukelmann, A. Brenes, L. Spinelli, L. V. Sinclair, A. I. Lamond, and D. A.
491 Cantrell. 2019. Quantitative analysis of T cell proteomes and environmental sensors
492 during T cell differentiation. *Nat Immunol* 20: 1542-1554.
493 Hughes, C. S., S. Foehr, D. A. Garfield, E. E. Furlong, L. M. Steinmetz, and J. Krijgsveld. 2014.
494 Ultrasensitive proteome analysis using paramagnetic bead technology. *Mol Syst Biol*
495 10: 757.
496 Hukelmann, J. L., K. E. Anderson, L. V. Sinclair, K. M. Grzes, A. B. Murillo, P. T. Hawkins, L. R.
497 Stephens, et al. 2016. The cytotoxic T cell proteome and its shaping by the kinase
498 mTOR. *Nat Immunol* 17: 104-112.
499 Jackson, L. J., J. A. Pheneger, T. J. Pheneger, G. Davis, A. D. Wright, J. E. Robinson, S. Allen, et
500 al. 2012. The role of PIM kinases in human and mouse CD4+ T cell activation and
501 inflammatory bowel disease. *Cell Immunol* 272: 200-213.
502 James, O. J., M. Vandereyken, J. M. Marchingo, F. Singh, S. E. Bray, J. Wilson, A. G. Love, and
503 M. Swamy. 2021. IL-15 and PIM kinases direct the metabolic programming of
504 intestinal intraepithelial lymphocytes. *Nat Commun* 12: 4290.
505 Kalia, V., and S. Sarkar. 2018. Regulation of Effector and Memory CD8 T Cell Differentiation by
506 IL-2-A Balancing Act. *Front Immunol* 9: 2987.
507 Knudson, K. M., C. J. Pritzl, V. Saxena, A. Altman, M. A. Daniels, and E. Teixeiro. 2017.
508 NFkappaB-Pim-1-Eomesodermin axis is critical for maintaining CD8 T-cell memory
509 quality. *Proc Natl Acad Sci U S A* 114: E1659-E1667.
510 Laird, P. W., N. M. van der Lugt, A. Clarke, J. Domen, K. Linders, J. McWhir, A. Berns, and M.
511 Hooper. 1993. In vivo analysis of Pim-1 deficiency. *Nucleic Acids Res* 21: 4750-4755.
512 Law, C. W., M. Alhamdoosh, S. Su, X. Dong, L. Tian, G. K. Smyth, and M. E. Ritchie. 2016. RNA-
513 seq analysis is easy as 1-2-3 with limma, Glimma and edgeR. *F1000Res* 5.
514 Lawrence, M., W. Huber, H. Pages, P. Aboyoun, M. Carlson, R. Gentleman, M. T. Morgan, and
515 V. J. Carey. 2013. Software for computing and annotating genomic ranges. *PLoS*
516 *Comput Biol* 9: e1003118.
517 Li, H., L. Xie, L. Zhu, Z. Li, R. Wang, X. Liu, Z. Huang, et al. 2022. Multicellular immune
518 dynamics implicate PIM1 as a potential therapeutic target for uveitis. *Nat Commun*
519 13: 5866.
520 Locard-Paulet, M., G. Voisinne, C. Froment, M. Goncalves Menoita, Y. Ounoughene, L. Girard,
521 C. Gregoire, et al. 2020. LymphoAtlas: a dynamic and integrated phosphoproteomic
522 resource of TCR signaling in primary T cells reveals ITSN2 as a regulator of effector
523 functions. *Mol Syst Biol* 16: e9524.
524 Maney, N. J., H. Lemos, B. Barron-Millar, C. Carey, I. Herron, A. E. Anderson, A. L. Mellor, et
525 al. 2021. Pim Kinases as Therapeutic Targets in Early Rheumatoid Arthritis. *Arthritis*
526 *Rheumatol* 73: 1820-1830.
527 Marchingo, J. M., L. V. Sinclair, A. J. Howden, and D. A. Cantrell. 2020. Quantitative analysis of
528 how Myc controls T cell proteomes and metabolic pathways during T cell activation.
529 *Elife* 9.
530 Matikainen, S., T. Sareneva, T. Ronni, A. Lehtonen, P. J. Koskinen, and I. Julkunen. 1999.
531 Interferon-alpha activates multiple STAT proteins and upregulates proliferation-
532 associated IL-2Ralpha, c-myc, and pim-1 genes in human T cells. *Blood* 93: 1980-
533 1991.

534 McCarthy, D. J., Y. Chen, and G. K. Smyth. 2012. Differential expression analysis of multifactor
535 RNA-Seq experiments with respect to biological variation. *Nucleic Acids Res* 40: 4288-
536 4297.
537 McCarthy, D. J., K. R. Campbell, A. T. Lun, and Q. F. Wills. 2017. Scater: pre-processing, quality
538 control, normalization and visualization of single-cell RNA-seq data in R.
539 *Bioinformatics* 33: 1179-1186.
540 Mikkers, H., M. Nawijn, J. Allen, C. Brouwers, E. Verhoeven, J. Jonkers, and A. Berns. 2004.
541 Mice deficient for all PIM kinases display reduced body size and impaired responses
542 to hematopoietic growth factors. *Mol Cell Biol* 24: 6104-6115.
543 Navarro, M. N., J. Goebel, J. L. Hukelmann, and D. A. Cantrell. 2014. Quantitative
544 phosphoproteomics of cytotoxic T cells to reveal protein kinase d 2 regulated
545 networks. *Mol Cell Proteomics* 13: 3544-3557.
546 Navarro, M. N., J. Goebel, C. Feijoo-Carnero, N. Morrice, and D. A. Cantrell. 2011.
547 Phosphoproteomic analysis reveals an intrinsic pathway for the regulation of histone
548 deacetylase 7 that controls the function of cytotoxic T lymphocytes. *Nat Immunol* 12:
549 352-361.
550 Nolz, J. C., G. R. Starbeck-Miller, and J. T. Harty. 2011. Naive, effector and memory CD8 T-cell
551 trafficking: parallels and distinctions. *Immunotherapy* 3: 1223-1233.
552 Peng, C., A. Knebel, N. A. Morrice, X. Li, K. Barringer, J. Li, S. Jakes, et al. 2007. Pim kinase
553 substrate identification and specificity. *J Biochem* 141: 353-362.
554 Peperzak, V., E. A. Veraar, A. M. Keller, Y. Xiao, and J. Borst. 2010. The Pim kinase pathway
555 contributes to survival signaling in primed CD8+ T cells upon CD27 costimulation. *J*
556 *Immunol* 185: 6670-6678.
557 Ricciardi, S., N. Manfrini, R. Alfieri, P. Calamita, M. C. Crosti, S. Gallo, R. Muller, et al. 2018.
558 The Translational Machinery of Human CD4(+) T Cells Is Poised for Activation and
559 Controls the Switch from Quiescence to Metabolic Remodeling. *Cell Metab* 28: 961.
560 Ritchie, M. E., B. Phipson, D. Wu, Y. Hu, C. W. Law, W. Shi, and G. K. Smyth. 2015. limma
561 powers differential expression analyses for RNA-sequencing and microarray studies.
562 *Nucleic Acids Res* 43: e47.
563 Robinson, M. D., D. J. McCarthy, and G. K. Smyth. 2010. edgeR: a Bioconductor package for
564 differential expression analysis of digital gene expression data. *Bioinformatics* 26:
565 139-140.
566 Rolf, J., M. Zarrouk, D. K. Finlay, M. Foretz, B. Viollet, and D. A. Cantrell. 2013. AMPKalpha1: a
567 glucose sensor that controls CD8 T-cell memory. *Eur J Immunol* 43: 889-896.
568 Saravia, J., J. L. Raynor, N. M. Chapman, S. A. Lim, and H. Chi. 2020. Signaling networks in
569 immunometabolism. *Cell Res* 30: 328-342.
570 Schatz, J. H., E. Oricchio, A. L. Wolfe, M. Jiang, I. Linkov, J. Maragulia, W. Shi, et al. 2011.
571 Targeting cap-dependent translation blocks converging survival signals by AKT and
572 PIM kinases in lymphoma. *J Exp Med* 208: 1799-1807.
573 Sinclair, L. V., D. Finlay, C. Feijoo, G. H. Cornish, A. Gray, A. Ager, K. Okkenhaug, et al. 2008.
574 Phosphatidylinositol-3-OH kinase and nutrient-sensing mTOR pathways control T
575 lymphocyte trafficking. *Nat Immunol* 9: 513-521.
576 Sinclair, L. V., A. J. Howden, A. Brenes, L. Spinelli, J. L. Hukelmann, A. N. Macintyre, X. Liu, et
577 al. 2019. Antigen receptor control of methionine metabolism in T cells. *Elife* 8.
578 Sollberger, G., A. J. Brenes, J. Warner, J. S. C. Arthur, and A. J. M. Howden. 2023. Quantitative
579 proteomics reveals tissue-specific, infection-induced and species-specific neutrophil

580 protein signatures. *bioRxiv* 10.1101/2023.09.05.556395 DOI:
581 2023.2009.2005.556395.
582 Spinelli, L., J. M. Marchingo, A. Nomura, M. P. Damasio, and D. A. Cantrell. 2021.
583 Phosphoinositide 3-Kinase p110 Delta Differentially Restrains and Directs Naive
584 Versus Effector CD8(+) T Cell Transcriptional Programs. *Front Immunol* 12: 691997.
585 Storey, J. D., A. J. Bass, A. Dabney, and D. Robinson. 2023. qvalue: Q-value estimation for
586 false discovery rate control, version R package version 2.32.0.
587 Suzuki, C., R. G. Garces, K. A. Edmonds, S. Hiller, S. G. Hyberts, A. Marintchev, and G. Wagner.
588 2008. PDCD4 inhibits translation initiation by binding to eIF4A using both its MA3
589 domains. *Proc Natl Acad Sci U S A* 105: 3274-3279.
590 Swamy, M., S. Pathak, K. M. Grzes, S. Damerow, L. V. Sinclair, D. M. van Aalten, and D. A.
591 Cantrell. 2016. Glucose and glutamine fuel protein O-GlcNAcylation to control T cell
592 self-renewal and malignancy. *Nat Immunol* 17: 712-720.
593 Tan, H., K. Yang, Y. Li, T. I. Shaw, Y. Wang, D. B. Blanco, X. Wang, et al. 2017. Integrative
594 Proteomics and Phosphoproteomics Profiling Reveals Dynamic Signaling Networks
595 and Bioenergetics Pathways Underlying T Cell Activation. *Immunity* 46: 488-503.
596 Warfel, N. A., and A. S. Kraft. 2015. PIM kinase (and Akt) biology and signaling in tumors.
597 *Pharmacol Ther* 151: 41-49.
598 Weninger, W., M. A. Crowley, N. Manjunath, and U. H. von Andrian. 2001. Migratory
599 properties of naive, effector, and memory CD8(+) T cells. *J Exp Med* 194: 953-966.
600 Wingett, D., A. Long, D. Kelleher, and N. S. Magnuson. 1996. pim-1 proto-oncogene
601 expression in anti-CD3-mediated T cell activation is associated with protein kinase C
602 activation and is independent of Raf-1. *J Immunol* 156: 549-557.
603 Wisniewski, J. R., M. Y. Hein, J. Cox, and M. Mann. 2014. A "proteomic ruler" for protein copy
604 number and concentration estimation without spike-in standards. *Mol Cell*
605 *Proteomics* 13: 3497-3506.
606 Zougman, A., P. J. Selby, and R. E. Banks. 2014. Suspension trapping (STrap) sample
607 preparation method for bottom-up proteomics analysis. *Proteomics* 14: 1006-1000.
608

609 **Acknowledgements:**
610 The authors thank members of the Cantrell group for their critical discussion of the data, in
611 particular we thank Linda Sinclair for critical reading and comments on the manuscript. We
612 thank Victor Tybulewicz for providing the Pim1-/- and Pim2-/- mice, E Emslie for help with
613 mouse maintenance and experimental support, B Stubbs for technical assistance with
614 mouse genotyping, A Brenes for assistance with analytical tools, A Gardner, A Rennie and R
615 Clarke from the Flow Cytometry facility for cell sorting, K Beattie and A Atrih from the
616 Fingerprint proteomics facility for performed mass spectrometry, S Thomson for assistance
617 with adoptive transfer experiments, the Biological Resource Unit at the University of
618 Dundee and the Finnish Functional Genomics Centre, University of Turku and Abo Akademi
619 Biocenter Finland for performing RNA sequencing. This research was supported by a
620 Wellcome Trust Principal Research Fellowship to DAC (205023/Z/16/Z), a Wellcome Trust
621 Equipment Award to DAC (202950/Z/16/Z), an EMBO Long term Fellowship (ALTF 1543–
622 2015) and NHMRC CJ Martin Early Career fellowship (APP1120748) to JMM and has received
623 funding from the European Union's Horizon 2020 research and innovation programme
624 under the Marie Skłodowska-Curie grant agreement No 705984 to JMM and DAC.
625

626 **Materials and Methods:**

627 **Mice**

628 Pim1$^{-/-}$ (Pim1 KO)(Laird et al., 1993) and Pim2$^{-/-}$ or Pim2$^{-/Y}$ (Pim2 KO) mice(Mikkers et al.,
629 2004) on the FVB/N background were backcrossed for >10 generations onto a C57BL/6
630 background and were a generous gift from Prof Victor Tybulewicz. Pim1 KO and Pim2 KO
631 mice were inter-crossed to generate the Pim1/Pim2 double KO (Pim dKO) strain. Pim dKO,
632 C57BL/6, Ly5.1, P14 and OT1 mice were bred and maintained in the WTB/RUTG, University
633 of Dundee in compliance with UK Home Office Animals (Scientific Procedures) Act 1986
634 guidelines. Mice used for proteomics and RNAseq studies were male and 12-15 weeks of
635 age. Age/sex matched mice were used for all other experiments between 5–52 weeks of
636 age, with most being between 10 – 20 weeks.

637

638 **Cell culture**

639 Single cell suspensions were generated by mashing mouse lymph nodes (brachial, axial,
640 inguinal, superficial cervical, deep cervical, lumbar) or spleens through a 70 µm strainer. Red
641 blood cells were lysed with Ack buffer (150 mM NH_4Cl 10 mM $KHCO_3$110 µM Na_2EDTA pH
642 7.8). Cells were cultured in RPMI 1640 containing glutamine (Invitrogen), supplemented
643 with 10% FBS (Gibco), penicillin/streptomycin (Gibco) and 50 µM β-mercaptoethanol
644 (Sigma) at 37 °C with 5% CO_2.

645

646 For 24 hour TCR activation WT and Pim dKO proteomics and phenotyping, lymph node
647 suspension from 2 mice per biological replicate were activated with 0.5 µg/mL anti-mouse
648 CD3 (Biolegend) and 0.5 µg/mL anti-mouse CD28 (eBioscience) in 2 × 10 mL complete
649 culture medium in six well plates. Proteomics samples were generated in biological
650 triplicate.

651

652 For generation of memory-like or effector cytotoxic T lymphocytes (CTL) from mice with
653 polyclonal T cell repertoires, LN or spleen single cell suspensions were activated with 0.5
654 µg/mL anti-mouse CD3 (Biolegend) and 0.5 µg/mL anti-mouse CD28 (eBioscience) and
655 recombinant human IL-15 (20 ng/mL, Peprotech) or recombinant human IL-2 (20 ng/mL,
656 Proleukin, Novartis) in 10 mL complete culture medium per organ per mouse. After 2 days
657 of activation (~40 hours) cells were washed out of activation medium and resuspended at

658 0.3 million T cells/mL in fresh culture medium and cytokine 20 ng/mL of IL-15 or IL-2 for
659 memory-like and effector T cells respectively. T cells were subsequently split into fresh
660 medium and cytokine daily at a density of 0.5 million/ mL and 0.3 million/mL for memory-
661 like and effector T cells respectively until analysis timepoint.
662
663 For generation of effector CTL from TCR-transgenic P14 mice LN single cell suspensions were
664 activated with 100 ng/mL gp33 peptide, recombinant human IL-2 (20 ng/mL) and
665 recombinant mouse IL12 (2 ng/mL) (Peprotech) for 2 days, before washing out of activation
666 media and splitting cells daily into fresh media containing IL-2 (20 ng/mL) at a density of 0.3
667 million/mL.
668
669 For co-culture experiments Ly5.1+ WT and Pim dKO (Ly5.2+) cell suspensions were mixed in
670 a 50:50 ratio based on total T cell numbers before activation. A portion of the mixed naïve T
671 cells maintained in recombinant mouse IL-7 (5 ng/mL, Peprotech) to verify baseline T cell
672 ratios over time in culture.
673
674 For experiments where a pure CD8+ CTL population were required from non-TCR transgenic
675 mice (adoptive transfer, proteomics and RNAseq experiments), CD4 T cells were depleted
676 on day 3 of CTL cultures (i.e. 24 hours after being washed out of initial activation conditions)
677 by negative magnetic selection. T cells were resuspended in MACS buffer (PBS, 1mM EDTA,
678 2%FBS) at 10^8/mL, blocked with 50 µL/mL Rat Serum, incubated for 10 min with anti-CD4
679 biotin antibody (5 µg/mL, Biolegend), incubated for 5 min with 125 µL/mL RapidSphere
680 beads (StemCell Technologies), then volume topped up to 2.5 mL and placed in EasySep
681 magnet for 2.5 min. Supernatant containing CD8 T cells was collected and returned to
682 culture as per CTL protocol above. CD4 T cell depletion was confirmed by flow cytometry,
683 with CD4+ cells making up <0.4% of live cells.
684
685 In experiments where cytokine was withdrawn T cells were washed at least twice with warm
686 complete medium. Where indicated CTL were treated with 100 nM Tofacitinib
687 (Selleckchem), 20 nM of rapamycin (Merck), 20 ng/mL PDBu (Cell Signaling Technologies)
688 and ionomycin 500 ng/mL (Merck) or the pan PIM kinase inhibitors PIM447 (1 or 5 µM as
689 indicated) and AZD1208 (1 or 10 µM as indicated) (both Medchemexpress).

690 **Flow cytometry**

691 Flow cytometry data was acquired on a FACSVerse using FACSuite software, FACSCanto, or
692 LSR II Fortessa with FACS DIVA software (BD Biosciences) or Novocyte (Acea Biosciences
693 Inc.) with NovoExpress software (Agilent). Data was analysed using Flowjo software version
694 9.9.6 or version 10.6.1 and above (Treestar).

695 Cell surface staining antibodies conjugated to BV421, BV510, V500, FITC, PE, PerCPCy5.5,
696 PECy7, APC, A647 and APCeF780 were obtained from BD Biosciences, eBioscience or
697 Biolegend. Fc receptors were blocked using Fc block (BD Biosciences). Antibody staining for
698 surface markers was performed at 1:200 in PBS 1%FBS. Antibody clones were as follows:
699 CD4 (RM4-5), CD8 (53–6.7), CD25 (7D4 or PC61), CD44 (IM7), CD45.1 (A20), CD45.2 (104),
700 CD62L (MEL-14), CD69 (H1.2F), CD71 (RI7217), TCRbeta (H57-597).

701

702 For IFNγ and Granzyme B intracellular staining cells were fixed and permeabilised using
703 eBioscience Intracellular Fixation and Permeabilisation kit (eBioscience) as per manufacturer
704 instructions. Cells were stained with anti-IFNγ (XMG1.2) and anti-Granzyme B (NGZB) at
705 1:100 and 1:200 respectively. For intracellular IFNγ staining GolgiPlug (BD) was added to the
706 culture 4 hours prior to analysis.

707 For intracellular phospho S6 staining cells were fixed with 0.5% paraformaldehyde at 37 ^{o}C
708 and permeabilised with ice cold 90% methanol. Cells were stained at 1:100 with anti-
709 phospho S6 ribosomal protein (Ser235/236) Alexa Fluor 647 (D57.2.2E, Cell Signaling
710 Technologies cat#4851S).

711 For intracellular phospho-STAT5 staining cells were fixed with 1% paraformaldehyde at
712 room temperature and permeabilised with ice cold 90% methanol. Cells were stained at
713 1:200 with rabbit anti-phospho STAT5 (Y694) (C11C5, Cell Signaling Technologies cat#9359S)
714 followed by anti-rabbit IgG Fab2 Alexa Fluor 647 (Cell Signaling Technologies cat#4414S).

715 For intracellular PDCD4 staining cells were fixed with 1% paraformaldehyde at room
716 temperature and permeabilised with Perm Buffer (eBioscience, cat# 00-8333-56). Cells were
717 stained at 1:100 with rabbit anti-PDCD4 (D29C6, Cell Signaling Technologies cat#9535S)
718 followed by anti-rabbit IgG Fab2 Alexa Fluor 647 (Cell Signaling Technologies cat#4414S).

719

720

721

722 **Cell sorting**

723 Cell sorting was performed on a Sony SH800S cell sorter (Sony Biotechnology). Staining was
724 performed in PBS 1% FBS and sorting and collection of cells for proteomics analysis was
725 performed in RPMI 1640 containing glutamine, supplemented with 1% FBS. 24 hour TCR
726 activated WT and Pim dKO CD4 and CD8 T cells were sorted as: DAPI-CD69+ CD8+ or CD4+.
727 Cells were washed twice with HBSS (no calcium, no magnesium, no phenol red, GIBCO)
728 before being snap frozen in liquid nitrogen and stored at −80°C until further processing.
729

730 **CTL number estimation and viability**

731 Absolute CD8 T cell number per well/flask and % live cells was assessed in CTL cultures by
732 volumetric measurement of cell number from 50 µL culture medium. Cells were transferred
733 into 450 µL PBS containing low concentration anti-CD8, anti-CD4 antibody (both 1:1500) and
734 DAPI (1 µg/mL, Thermofisher Scientific) or propidium iodide (0.2 µg/mL, Sigma) and cell
735 number and viability assessed on either FACSVerse or Novocyte flow cytometers. Estimated
736 live cell counts were corrected for assay dilution ratio, total culture volume and splitting
737 ratios for each time point. Proportions of CD8 T cells that were Ly5.1+ or Ly5.2+ from
738 parallel surface staining were used to calculate WT and Pim dKO numbers respectively in co-
739 culture experiments.
740

741 **CTV proliferation assay**

742 For CTV proliferation assay, lymph node suspensions at 10^7 cells per mL in PBS 0.5%FCS
743 were labelled with 5 µM CTV (Invitrogen) for 20 min at 37°C before reaction was quenched
744 and cells washed with cold medium. 10^5 live cells were activated with αCD3/αCD28 (both
745 0.5 µg/mL) or maintained in IL-7 (5 ng/mL) +/- rapamycin (20 nM) in 200 µL total volume in
746 96 well flat-bottomed plates. Propidium iodide (0.2 µg/mL), low dose αCD4, αCD8 antibody
747 (both 1:3200 final concentration) and 10,000 sphero rainbow beads (BD) were added to
748 wells prior to analysis of beads number, cell number, cell viability, CD4 and CD8 T cell
749 composition and CTV profile of samples by flow cytometry. The ratio between the known
750 number of beads added to the number of beads measured per well was multiplied with the
751 number of cells measured to calculate the absolute cell number per well. Cell number per
752 division was then corrected for the effect of expansion by dividing cell number per division

753 by 2^division number and the arithmetic mean division number calculated from these
754 values.
755
756 **Protein synthesis assay**
757 To assess protein synthesis cells were cultured with 20 µM O-propargyl puromycin (OPP,
758 Jena Bioscience) for 10 min. Control cells were cultured with cycloheximide (100 µg/mL,
759 Sigma-Aldrich) for 20 min prior to addition of OPP to assess background staining level when
760 cytosolic protein synthesis is completely inhibited. Cells were washed, fixed with 1% PFA,
761 permeabilised with 0.5% Triton x-100 and OPP incorporation into newly synthesised
762 peptides was measured by conjugating with Alexa647-azide via a Click-IT chemistry reaction
763 (2 µM Alexa-647-azide, 2 mM $CuSO_4$, 5 mM ascorbic acid in PBS) (Invitrogen) and assessing
764 fluorescence by flow cytometry.
765
766 **Adoptive Transfer**
767 WT and Pim dKO CD8 T cells were activated and expanded in IL-2 as described above. On
768 day 6 of culture WT and Pim dKO CTL were labelled with either CTV, or 5 µM CFSE
769 (Invitrogen) as per CTV assay protocol described above, with the exception that labelling
770 was performed in RPMI 1640 and CFSE labelling was for 10 min. CTV and CFSE labelling was
771 alternated between genotypes across biological replicates to prevent any potential
772 introduction of bias due to possible differences in dye toxicity. Labelled WT and Pim dKO
773 CD8 T cells were mixed in a 50:50 ratio and 5 million cells/mouse were adoptively
774 transferred via intravenous tail injection into C57BL/6 recipient mice. Recipient mice were
775 sacrificed and blood, spleen and lymph nodes (axillary, brachial and inguinal) removed 4 and
776 23 hours post-transfer and the ratio of CTV to CFSE cells assessed by flow cytometry.
777
778 **Western blotting**
779 Cell pellets were lysed in RIPA buffer (100 mM HEPES, pH 7.4, 150 mM NaCl, 1% NP40, 0.1%
780 SDS, 0.5% sodium deoxycholate, 10% glycerol, 1 mM EDTA, 1 mM EGTA, 1 mM TCEP, and
781 protease and phosphatase inhibitors (Roche)) at 20 million T cells/mL at 4 ^{o}C. Lysates were
782 sonicated, centrifuged 12 min, 13,000 rpm, 4°C. Supernatant was transferred to fresh tube
783 and NuPAGE LDS sample buffer (1×) (Life Technologies) and tris(2-carboxyethyl)phosphine
784 (TCEP, 25mM, Thermofisher) was added before boiling samples at 100°C for 3 min. Samples

785 were loaded and separated by SDS-PAGE (NuPAGE 4-12% gradient precast gels
786 (ThermoFisher) or 12% polyacrylamide running gel), and then transferred to nitrocellulose
787 membranes (Whatman). Equal cell numbers (~140,000 cells) were loaded per lane. Blots
788 were probed with the following primary antibodies: S6K (5G10, Cell Signaling Technology,
789 cat# 2217S), S6K p-T389 (108D2, Cell Signaling Technology, cat# 9234S), STAT5 p-Y694
790 (C11C5, Cell Signalling Technology, cat# 9359S), Pim1 (12H8, Santa Cruz, cat# SC-13513),
791 Pim2 (1D12, Santa Cruz, cat# SC-13514). Horseradish peroxidase (HRP)-conjugated anti-
792 rabbit or anti-mouse secondary antibodies were used to assess protein signal (Thermo
793 Scientific, Cell Signaling Technologies). Chemiluminescence was measured using an Odyssey
794 Fc Imaging System (Licor) and Image Studio Software (LI-COR) was used to quantify
795 chemiluminescence.
796
797 **Proteomics:**
798 **Proteomics sample preparation**
799 Cell pellets for 24 hour TCR WT and Pim dKO CD4 and CD8 T cells were activated and sorted
800 as described above.
801
802 IL-2 and IL-15 expanded WT and Pim dKO CD8 T cells on day 6 of culture days, were cultured
803 in fresh warm complete medium and cytokine for 2 hours before cells were harvested,
804 washed twice in ice-cold HBSS and cell pellets snap frozen in liquid nitrogen. Duplicate cell
805 pellets were collected per sample for parallel processing for proteomics or RNAseq analysis.
806
807 IL-2 expanded P14 CD8 T cells on day 5 of culture were treated for 24 hours with PIM447 (5
808 µM) or AZD1208 (10 µM). Cells were harvested on day 6 of culture, washed twice in ice-cold
809 HBSS and cell pellets snap frozen in liquid nitrogen.
810
811 For all proteomics samples, cell pellets were lysed in 4% SDS, 50 mM TEAB pH 8.5, 10 mM
812 TCEP (5 min, 1200 rpm, room temperature), boiled (5 min, 500 rpm, 95 ^{o}C), then sonicated
813 with a BioRuptor (30 s on, 30 s off x30 cycles). Protein concentration was determined using
814 EZQ protein quantitation kit (Invitrogen) as per manufacturer instructions. Lysates were
815 alkylated with 20 mM iodoacetamide (Sigma) for 1 hr at room temperature in the dark.

816 24 hour TCR WT and Pim dKO CD4 and CD8 T cell proteomics samples and Day 6, 24 hour
817 pan-PIM kinase inhibitor treated IL2 expanded CD8 T cell samples were cleaned up and
818 peptides generated by an SP3 bead protocol(Hughes et al., 2014) as described
819 previously(Marchingo et al., 2020). As outlined in reference(Marchingo et al., 2020):
820 "Briefly, 200 µg of 1:1 mixed Hydrophobic and Hydrophilic Sera-Mag SpeedBead
821 Carboxylate-Modified Magnetic Particles were added per protein sample then acidified
822 to ~pH 2.0 by addition 10:1 Acetonitrile: Formic Acid. Beads were immobilised on a
823 magnetic rack and proteins washed with 2 × 70% ethanol and 1 × 100% acetonitrile. Rinsed
824 beads were reconstituted in 0.1% SDS 50 mM TEAB pH 8.5, 1 mM CaCl2 and digested
825 overnight with LysC followed by overnight digestion with Trypsin, each at a 1:50 enzyme to
826 protein ratio. Peptide clean up was performed as per SP3 procedure(Hughes et al., 2014).
827 Briefly, protein-bead mixtures were resuspended and 100% acetonitrile added for 10 min
828 (for the last 2 min of this beads were immobilised on a magnetic rack). Acetonitrile and
829 digest buffer were removed, peptides were washed with acetonitrile and eluted in 2%
830 DMSO. Peptide concentration was quantified using CBQCA protein quantitation kit
831 (Invitrogen) as per manufacturer protocol. Formic acid was added to 5% final
832 concentration".
833
834 24 hour TCR WT and Pim dKO CD4 and CD8 T cell proteomics samples were fractionated
835 using high pH reverse phase liquid chromatography as described previously(Marchingo et
836 al., 2020). As outlined in reference(Marchingo et al., 2020): "Samples were loaded onto a
837 2.1 mm x 150 mm XBridge Peptide BEH C18 column with 3.5 µm particles (Waters). Using a
838 Dionex Ultimate3000 system, the samples were separated using a 25 min multistep gradient
839 of solvents A (10 mM formate at pH 9 in 2% acetonitrile) and B (10 mM ammonium formate
840 pH 9 in 80% acetonitrile), at a flow rate of 0.3 mL/min. Peptides were separated into 16
841 fractions which were consolidated into eight fractions. Fractionated peptides were dried in
842 vacuo then dissolved in 5% Formic Acid for analysis by LC-ES-MS/MS".
843 24 hour pan-PIM kinase inhibitor treated day 6 IL2 expanded CD8 T cell samples, were not
844 fractionated. They were dried in vacuo then dissolved in 5% Formic Acid for analysis by LC-
845 ES-MS/MS after SP3 cleanup.
846

847 Day 6 IL-2 and IL-15 expanded WT and PimdKO CD8 T cells samples were cleaned up and
848 peptides generated by an S-Trap protocol (Zougman et al., 2014) as per manufacturer
849 protocol (Protifi). Briefly, add phosphoric acid (to final concentration 1.2%) then S-Trap
850 binding buffer (90% methanol, 100 mM TEAB, pH 7.1) at a ratio 1:7 v:v lysate:binding buffer
851 was added to sample lysates containing 100-300 µg total protein. Acidified lysates were
852 loaded to S-Trap mini columns and spun (4,000 g, 30 s) until all SDS lysate/S-Trap buffer had
853 passed through the column. Proteins were digested on column in digest buffer (50 mM
854 sodium bicarbonate) containing Trypsin at a 1:20 enzyme to protein ratio (2 hrs, 47°C
855 without shaking). Peptides were eluted by spinning in digest buffer (1000g, 1 min), then
856 0.2% aqueous formic acid (1000g, 1 min), then 50% acetonitrile 0.2% formic acid (4000g, 1
857 min). Peptide concentration was quantified using CBQCA protein quantitation kit
858 (Invitrogen) as per manufacturer protocol. Peptides were dried in vacuo then dissolved in
859 5% Formic Acid for analysis by LC-ES-MS/MS.
860
861 **Liquid chromatography electrospray tandem mass spectrometry analysis (LC-ES-MS/MS)**
862 ≤1 µg of peptide was analysed per fraction by Data-Dependent Acquisition (DDA) Mass
863 Spectrometry for 24 hour TCR WT and Pim dKO CD4 and CD8 T cell proteomics samples.
864 For label-free DDA proteomics of WT and Pim dKO CD4 and CD8 24 hour TCR activated T
865 cells samples were analysed as described previously(Sinclair et al., 2019). As outlined in
866 reference(Sinclair et al., 2019): "samples were injected onto a nanoscale C18 reverse-phase
867 chromatography system (UltiMate 3000 RSLC nano, Thermo Scientific) then electrosprayed
868 into an Orbitrap mass spectrometer (LTQ Orbitrap Velos Pro; Thermo Scientific). For
869 chromatography buffers were as follows: HPLC buffer A (0.1% formic acid), HPLC buffer B
870 (80% acetonitrile and 0.08% formic acid) and HPLC buffer C (0.1% formic acid). Peptides
871 were loaded onto an Acclaim PepMap100 nanoViper C18 trap column (100 µm inner
872 diameter, 2 cm; Thermo Scientific) in HPLC buffer C with a constant flow of 10 µl/min. After
873 trap enrichment, peptides were eluted onto an EASY-Spray PepMap RSLC nanoViper, C18, 2
874 µm, 100 Å column (75 µm, 50 cm; Thermo Scientific) using the buffer gradient: 2% B (0 to 6
875 min), 2% to 35% B (6 to 130 min), 35% to 98% B (130 to 132 min), 98% B (132 to 152 min),
876 98% to 2% B (152 to 153 min), and equilibrated in 2% B (153 to 170 min) at a flow rate of 0.3
877 µl/min. The eluting peptide solution was automatically electrosprayed using an EASY-Spray
878 nanoelectrospray ion source at 50° and a source voltage of 1.9 kV (Thermo Scientific) into

879 the Orbitrap mass spectrometer (LTQ Orbitrap Velos Pro; Thermo Scientific). The mass
880 spectrometer was operated in positive ion mode. Full-scan MS survey spectra (mass/charge
881 ratio, 335 to 1800) in profile mode were acquired in the Orbitrap with a resolution of
882 60,000. Data were collected using data- dependent acquisition: the 15 most intense peptide
883 ions from the preview scan in the Orbitrap were fragmented by collision-induced
884 dissociation (normalized collision energy, 35%; activation Q, 0.250; activation time, 10 ms) in
885 the LTQ after the accumulation of 5000 ions. Precursor ion charge state screening was
886 enabled, and all unassigned charge states as well as singly charged species were rejected.
887 The lock mass option was enabled for survey scans to improve mass accuracy. (Using Lock
888 Mass of 445.120024)".
889
890 ~0.2 µg of peptide was analysed per sample by single shot DDA Mass Spectrometry for 24
891 hour pan-PIM kinase inhibitor treated, day 6 IL2 expanded CD8 T cell samples.
892 Samples were injected onto a nanoscale C18 reverse-phase chromatography system
893 (UltiMate 3000 RSLC nano, Thermo Scientific) then electrosprayed into a Q-Exactive HF
894 (Thermo Scientific). A 2- 35% B gradient comprising of eluent A (0.1% formic acid) and
895 eluent B (80% acetonitrile/0.1% formic acid) was used to run a 120-minute gradient per
896 sample. With the mass spectrometer in positive mode the top 20 most intense peaks from a
897 mass range of 335-1800 m/z in each MS1 scan with a resolution of 60,000 were then taken
898 for MS2 analysis at a resolution of 15,000. Spectra were fragmented using Higher-energy C-
899 trap dissociation (HCD).
900
901 2 µg of peptide was analysed per sample by Data-Independent Acquisition (DIA) Mass
902 Spectrometry for the IL-2 and IL-15 expanded CD8 T cell proteomics samples. For label-free
903 DIA proteomics of Day 6 IL-2 and IL-15 expanded WT and Pim dKO CD8 T cells peptide samples
904 were analysed as described in (Sollberger et al., 2023) with some minor differences. Peptides
905 were injected onto a nanoscale C18 reverse-phase chromatography system (UltiMate 3000
906 RSLC nano, Thermo Scientific) then electrosprayed into an Orbitrap Exploris 480 Mass
907 Spectrometer (Thermo Scientific). For liquid chromatography buffers were as follows: buffer
908 A (0.1% formic acid in Milli-Q water (v/v)) and buffer B (80% acetonitrile and 0.1% formic acid
909 in Milli-Q water (v/v). Sample were loaded at 10 µL/min onto a trap column (100 µm × 2 cm,
910 PepMap nanoViper C18 column, 5 µm, 100 Å, Thermo Scientific) equilibrated in 0.1%

911 trifluoroacetic acid (TFA). The trap column was washed for 3 min at the same flow rate with
912 0.1% TFA then switched in-line with a Thermo Scientific, resolving C18 column (75 µm × 50
913 cm, PepMap RSLC C18 column, 2 µm, 100 Å). The peptides were eluted from the column at a
914 constant flow rate of 300 nl/min with a linear gradient from 3% buffer B to 6% buffer B in 5
915 min, then from 6% buffer B to 35% buffer B in 115 min, and finally to 80% buffer B within 7
916 min. The column was then washed with 80% buffer B for 4 min and re-equilibrated in 3%
917 buffer B for 15 min. Two blanks were run between each sample to reduce carry-over. The
918 column was kept at a constant temperature of 40°C.
919 The data was acquired using an easy spray source operated in positive mode with spray
920 voltage at 2.1 kV and the ion transfer tube temperature at 275°C. The MS was operated in
921 DIA mode. A scan cycle comprised a full MS scan (m/z range from 350-1650, with RF lens at
922 40%, AGC target set to custom, normalised AGC target at 300%, maximum injection time
923 mode set to custom, a maximum ion injection time of 20 ms, microscan set to 1 and source
924 fragmentation disabled. MS survey scan was followed by MS/MS DIA scan events using the
925 following parameters: multiplex ions set to false, collision energy mode set to stepped,
926 collision energy type set to normalized, HCD collision energies set to 25.5, 27 and 30%,
927 orbitrap resolution 30000, first mass 200, RF lens 40%, AGC target set to custom, normalized
928 AGC target 3000%, microscan set to 1 and maximum injection time 55 ms. Data for both MS
929 scan and MS/MS DIA scan events were acquired in profile mode.
930
931 **Proteomics data analysis**
932 The 24 hour TCR WT and Pim dKO CD4 and CD8 T cell DDA proteomics data and 24 hour
933 pan-PIM kinase inhibitor treated Day 6 IL2 expanded CD8 T cell DDA proteomics data were
934 processed, searched and quantified with the MaxQuant software package, version
935 1.6.10.43. For the protein and peptide searches we generated a hybrid database consisting
936 of all manually annotated mouse SwissProt entries, combined with mouse TrEMBL entries
937 with protein level evidence available and a manually annotated homologue within the
938 human SwissProt database as described in (Marchingo et al., 2020). For the 24 hour TCR
939 activated data this was from the Uniprot release 2020_06, for the 24 hour PIM kinase
940 inhibitor data this was from the Uniprot release 2019_08. Search parameters were as
941 described in (Marchingo et al., 2020): “The following MaxQuant search parameters were
942 used: protein N-terminal acetylation, methionine oxidation, glutamine to pyroglutamate,

943 and glutamine and asparagine deamidation were set as variable modifications and
944 carbamidomethylation of cysteine residues was selected as a fixed modification; Trypsin and
945 LysC were selected as the enzymes with up to two missed cleavages permitted; the protein
946 and PSM false discovery rate was set to 1%; matching of peptides between runs was
947 switched off".
948 Data filtering and protein copy number quantification was performed in the Perseus
949 software package, version 1.6.6.0. Proteins were quantified from unique peptides and razor
950 peptides (peptides assigned to a group, but not unique to that group). The data set was
951 filtered to remove proteins categorised as 'contaminants', 'reverse' and 'only identified by
952 site'.
953 To generate a point of reference between TCR activated WT and Pim dKO and inactive T
954 cells, naïve WT CD4 and CD8 T cell data from (Marchingo et al., 2020), which was collected
955 and processed identically, was included in proteomics search, results table and plot of
956 protein content. At this point biological replicate 3 from Pim dKO CD4 T cells was excluded
957 from further analysis due to poor sample quality (e.g. protein sequence coverage was an
958 average of 13.9% compared to an average of 18.2-24.6% for all other samples and
959 estimated total protein content per cell was ~1/3rd of that observed in the other two
960 biological replicates for that condition, despite no obvious difference in FSC measured when
961 FACS sorting).
962
963 The day 6 IL-2 and IL-15 expanded WT and Pim dKO CD8 T cell DIA proteomics data files were
964 searched using Spectronaut version 14.7. Data was analysed using a library-free approach.
965 Raw proteomics data files were searched using the Pulsar tool within Spectronaut using the
966 following settings: 0.01 FDR at the protein and peptide level with digest rule set to 'Trypsin'P'.
967 A maximum of two missed cleavages and minimum peptide length of 7 amino acids was
968 selected. Carbamidomethyl of cysteine was selected as a fixed modification while protein n-
969 terminal acetylation and methionine oxidation were selected as variable modifications.
970 Manufacturer default settings were used for identification, with protein and precursor q-
971 value set to 0.01 using default decoy strategy. For quantification settings, the MS-Level
972 quantity was set to 'MS2', major group Top N and minor group Top N were set as 'False' and
973 profiling was set as 'False'. The data was searched against the same mouse Uniprot database
974 as used above for DDA analysis.

975

976 Data was filtered to only include proteins for which at least one condition had peptides
977 detected in ≥2 biological replicates for 24 hour TCR and day 6 IL2 and IL15 WT and Pim dKO
978 data. Data was filtered to only include proteins for which at least two conditions had
979 peptides detected in ≥2 biological replicates for PIM kinase inhibitor data. Mean copy
980 number per cell was calculated using the "proteomic ruler' plugin as described in
981 (Wisniewski et al., 2014).
982 Mass contribution of proteins (g/cell) was calculated as (protein copy number) * (molecular
983 weight (Daltons)) / (Avogadro's constant). Differential expression analysis of protein copy
984 number was performed using RStudio (version 1.2.5033). P-values and fold-change were
985 calculated with the Bioconductor package Limma (version 3.44.3). Q-values were calculated
986 using Bioconductor package qvalue (version 2.20.0).
987
988 All scripts used to perform analysis are available from authors upon request.
989
990 **RNAseq:**
991 **RNA extraction and library preparation and RNA sequencing:**
992 Biological triplicate cell pellets of day 6 IL-2 or IL-15 differentiated CD8 T cells were collected
993 in parallel with proteomics samples as described above. Total RNA was extracted from cell
994 pellets with Qiagen RNAeasy mini kit (Qiagen) as per manufacturer instructions.
995 2 µg of RNA was submitted per sample to the Finnish Functional Genomics Centre, University
996 of Turku and Åbo Akademi University for library preparation and sequencing. RNA quality was
997 verified using Agilent Bioanalyzer 2100 or Advanced Analytical Fragment Analyzer. 300 ng of
998 total RNA was used for library preparation using the Illumina TruSeq Stranded mRNA sample
999 preparation kit (15031047) as per manufacturer instructions. Library quality was confirmed
1000 with Advanced Analytical Fragment Analyzer and quantified with Qubit Fluorometric
1001 Quantitation (Life Technologies). Sample libraries were pooled and run in a single lane on an
1002 Illumina NovaSeq 6000 with read length 2x 50 bp. Base calling was performed with bcl2fastq2
1003 conversion software (NovaSeq 6000) and automatic adapter trimming performed for fastq
1004 raw read files generated.
1005
1006

1007 **RNAseq data analysis**

1008 Quality assessment of raw reads was evaluated using MultiQC (Ewels et al., 2016). Raw reads
1009 were aligned to the GRCm38.p6 (Ensembl) build of the Mus musculus reference genome using
1010 the STAR aligner (Dobin et al., 2013) (version 2.7.1a), with 'outFilterType BySJout' option
1011 switched on to reduce spurious junctions. The STAR quantMode GeneCounts option was used
1012 to map aligned reads to genes to generate a gene counts matrix, using the annotation file
1013 GRCm38.101 (Ensembl).

1014

1015 Bioconductor package EdgeR (version 3.30.3) (Robinson et al., 2010; McCarthy et al., 2012)
1016 was used to reduce noise from low count genes with filterByExpr function and the resulting
1017 count matrix was normalised by the EdgeR Trimmed Mean of M-values (TMM) method.
1018 Differential expression analysis was performed using Limma package (version 3.44.3) (Ritchie
1019 et al., 2015; Law et al., 2016). Reads were converted to $\log_2$ counts per million and weighted
1020 using the voomWithQualityWeights function. A linear model was fitted to each gene and
1021 empirical Bayes moderated t-statistics were applied. q-values were calculated from using
1022 Bioconductor package qvalue (version 2.20.0) (Storey et al., 2023). The calculateTPM fuction
1023 from the Bioconductor package Scater (version 1.16.2) (McCarthy et al., 2017) was used to
1024 calculate TPM values for visualisation purposes, with total exon length calculated using
1025 GenomicRanges (version 1.40.0) (Lawrence et al., 2013) as the sum of the non-overlapping
1026 exonic regions for a gene.

1027

1028 **Combining Proteomics and RNAseq data**

1029 Proteomics data was annotated during Spectronaut search and Perseus analysis with Uniprot
1030 ID, MGI symbol and MGI ID information. BioMart (version 2.47.2) was used to extract UniProt
1031 identifiers, MGI symbols and MGI IDs for corresponding ENMUSG IDs of RNAseq data. RNAseq
1032 data was first combined with proteomics data based on UniProt ID. Proteins that didn't
1033 receive an initial match, were then combined by matching MGI ID values, then if still
1034 unmatched by MGI symbol. Data combinations were manually checked for obvious mis-
1035 annotations. Proteins with no corresponding mRNA identified or vice versa were excluded
1036 from the combined data file. In a few instances multiple proteins aligned to a single mRNA
1037 measurement or multiple mRNA aligned to a single protein measurement. For the purposes

1038 of this broad examination of how differences in expression at the protein or mRNA level these
1039 results were also excluded from the combined data table and subsequent analysis.
1040
1041 **Graphing and statistics**
1042 Heatmaps were generated using Broad Institute software Morpheus
1043 (https://software.broadinstitute.org/morpheus). Statistical tests performed for experiments
1044 other than proteomics and RNAseq are indicated in figure legends and were performed in
1045 Prism (GraphPad, version 9 or 10).
1046
1047 **Data availability**
1048 All data generated or analysed during this study are included in the manuscript and
1049 supporting files. Raw mass spec data files and MaxQuant or Spectronaut analysis files are
1050 available on the ProteomeXchange data repository and can be accessed with the following
1051 identifiers: PXD051198 for 24 hour TCR activated WT and Pim dKO CD4 and CD8 T cells;
1052 Naïve T cell data used as a point of reference for plotting 24 hour TCR proteomics has
1053 previously been published as part of (Marchingo et al., 2020) and can also be found under
1054 the identifier PXD016105; PXD051214 for Pim inhibitor proteomics; PXD051213 for day 6 IL-
1055 2 and IL-15 expanded WT and Pim dKO CD8 T cells. Raw RNAseq data files are available on
1056 the NCBI GEO website and can be accessed with the identifier GSE261667.

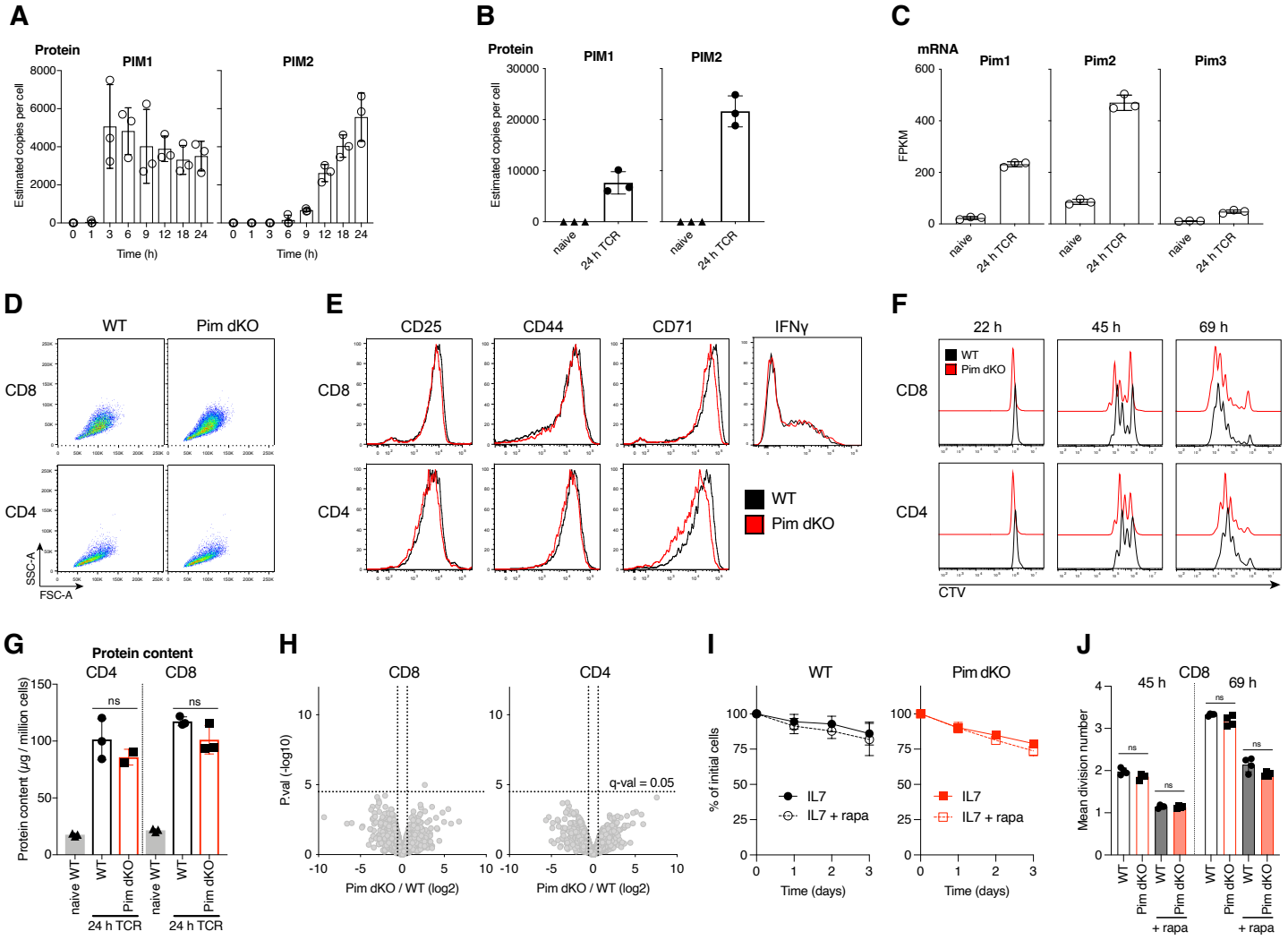

Figure 1. Pim1 and Pim2 are strongly TCR-induced, but dispensable for T cell activation

Estimated copies per cell of PIM1 and PIM2 protein from quantitative proteomics analysis of (**A**) OT1 CD8 T cells stimulated with SIINFEKL peptide for indicated times from published dataset (Marchingo et al., 2020) or (**B**) naïve ex vivo and 24 hour αCD3/αCD28 (TCR) activated WT CD8 T cells (see Fig 1G-H) for further details. (**C**) Fragments per kilobase million (FPKM) of *Pim1*, *Pim2* and *Pim3* mRNA from published (Spinelli et al., 2021) bulk RNAseq analysis of naïve and 24 hour gp33-41 peptide stimulated P14 CD8 T cells. Lymph node cell suspensions from C57BL/6 (WT) and *Pim1*KO/*Pim2*KO (Pim dKO) mice were activated for 24 hours with αCD3/αCD28 (both 0.5 µg/mL) and CD4 and CD8 T cell (**D**) FSC-A SSC-A profiles, (**E**) expression of surface activation markers (CD25, CD44, CD71) or CD8 T cell intracellular IFNγ were measured by flow cytometry. (**F**) Lymph node single cell suspensions from WT and Pim dKO mice were labelled with CellTrace Violet (CTV), activated with αCD3/αCD28 (both 0.5 µg/mL) and CD4 and CD8 T cell CTV proliferation profiles were measured at indicated time points. (G-H) Lymph node cell suspensions from WT and Pim dKO mice were stimulated for 24 hours with αCD3/αCD28 (both 0.5 µg/mL) and activated CD4 and CD8 T cells were sorted for analysis by quantitative proteomics. Data was analysed using proteomic ruler method (Wisniewski et al., 2014) to estimate protein copy number per cell. (**G**) Total protein content (µg/million cells) (one-way ANOVA), (**H**) Volcano plots of p-value ($-\log_{10}$) versus fold-change ($\log_2$) in protein copy number between Pim dKO and WT. Horizontal dotted line represents multi-test correction cut-off of q=0.05, vertical dotted line shows 1.5-fold change. Lymph node single cell suspensions from WT and Pim dKO mice were labelled with CellTrace Violet (CTV) and (**I**) cells were cultured in IL-7 (5ng/mL) +/- rapamycin (20 nM) and CD8 T cell numbers measured over time or (**J**) cells were activated with αCD3/αCD28 (both 0.5 µg/mL) +/- rapamycin (20 nM) and CD8 T cell mean division number was calculated over time (two-way ANOVA). Symbols in bar charts represent biological replicates, symbols in (I) represent the mean. Error bars show mean ± S.D. Flow cytometry dot plots and histograms are representative of (D-E) n = 3, except for IFNγ staining which is n=2 or show pooled data from (I) n=3-4 and (F, J) n=5 biological replicates, with data collected over at least 2 independent experiments. Quantitative proteomics was performed on biological triplicates.

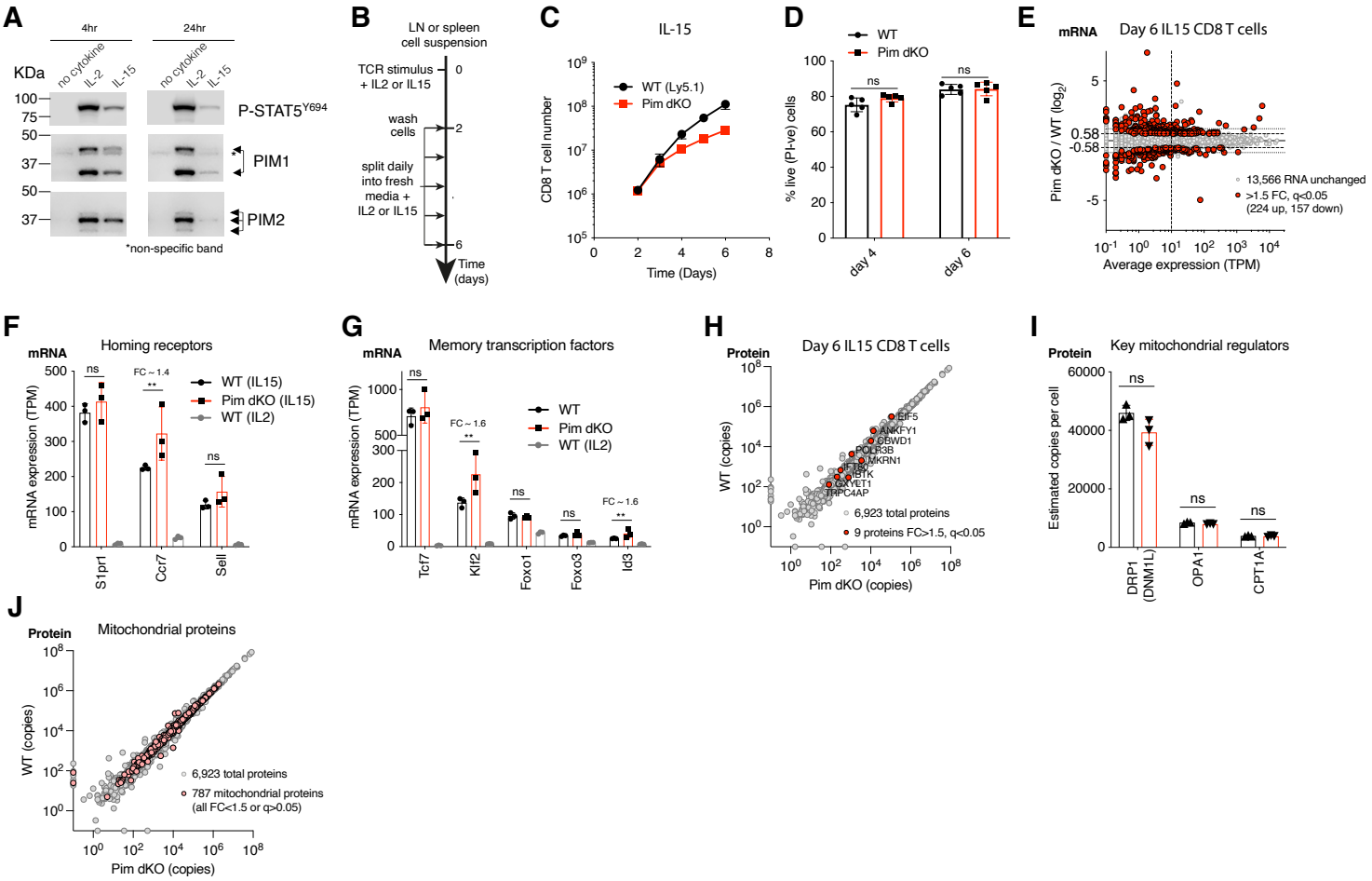

Figure 2. Pim1/Pim2 deficiency reduces IL-15-driven CD8 T cell proliferation but does not prevent memory differentiation.

(**A**) OT1 lymph node cell suspensions were SIINFEKL peptide activated for 36 hours, washed then cultured with no cytokine, IL-15 (20 ng/mL) or IL-2 (20 ng/mL) for 4 or 24 hours. Western blots of PIM1, PIM2 or pSTAT5 Y694 expression. (**B**) Schematic of cytokine driven memory and effector CD8 T cell expansion and differentiation cultures. Lymph node or spleen cell suspensions were activated for 2 days with TCR stimulus + cytokine, washed, then split daily into fresh media + cytokine. (**C**) WT (Ly5.1) and Pim dKO LN suspensions were mixed at a 50:50 ratio for T cells and cultured as outlined in (B) with TCR stimulus αCD3/αCD28 (both 0.5 µg/mL) + cytokine IL-15 (20 ng/mL), and CD8 T cell number was measured daily. (**D**) WT and Pim dKO T cells were expanded with IL-15 in separate cultures as per (B-C) and % live cells (PI-ve) were assessed on days 4 and 6 (two-way ANOVA). (E-J) WT and Pim dKO CD8 T cells were activated with TCR stimulus αCD3/αCD28 (both 0.5 µg/mL) + cytokine IL-15 (20 ng/mL), expanded with IL-15 as per (B), with an additional CD4 T cell magnetic depletion step on day 3 of culture. CD8 T cells were harvested on day 6 for parallel RNAseq and proteomic analysis. (**E**) Fold-change in mRNA expression between Pim dKO and WT versus average mRNA expression (TPM). mRNA expression (Transcripts per million, TPM) of (**F**) secondary lymphoid homing receptors Sell, Ccr7, S1pr1 and (**G**) key transcription factors involved in CD8 T cell memory differentiation and maintenance Tcf7, Klf2, Foxo1, Foxo3, Id3. (**H**) WT vs Pim dKO protein copy numbers, differentially expression proteins (FC>1.5, q<0.05) are highlighted in red (**I**) Protein copy numbers per cell for key mitochondrial proteins DRP1, OPA1 and CPT1A. (**J**) WT vs Pim dKO protein copy numbers, mitochondrial proteins (as defined in MitoCarta 3.0) are highlight in pink. Symbols in bar charts represent biological replicates, symbols in (C,H,J) represent the mean. Error bars show mean ± S.D. Data are representative of (A) n=3 or show pooled data from (C) n = 4, and (D) n=5 biological replicates with data collected over at least 2 independent experiments. Quantitative proteomics and RNAseq was performed on biological triplicates. ** q≤0.01, fold-change (FC) shown on bar graphs when q<0.05.

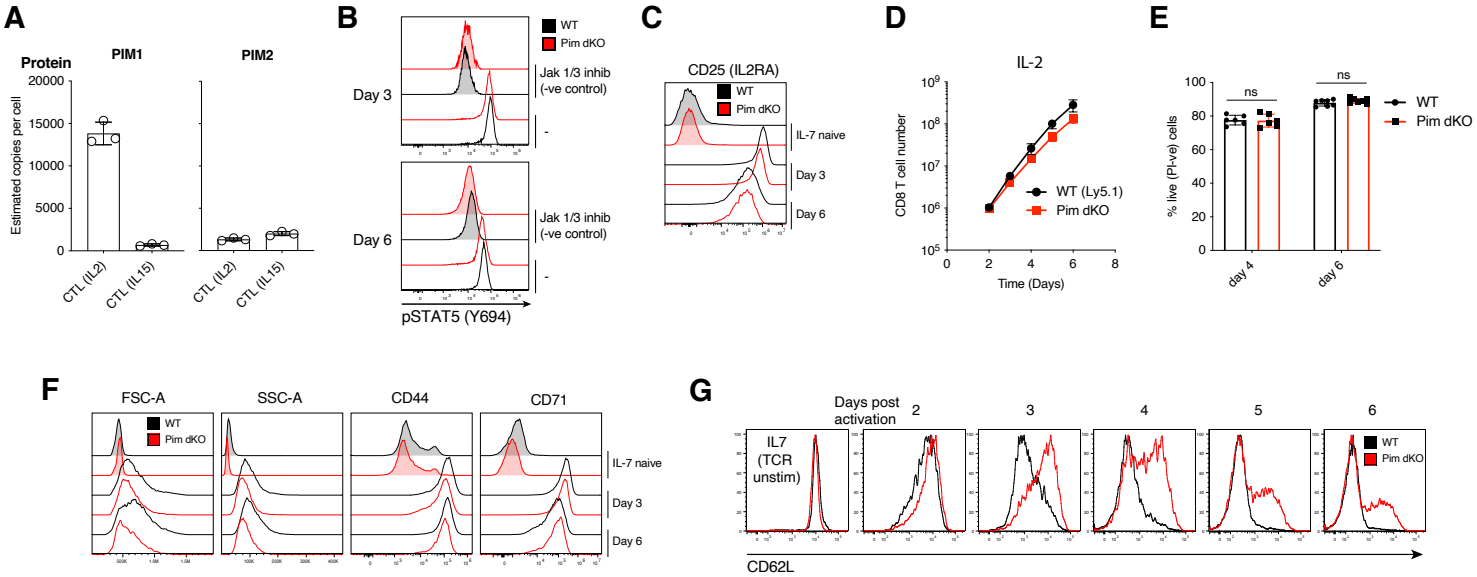

Figure 3. Pim dKO IL-2 differentiated effector T cells have reduced cell size and sustained expression of CD62L

(**A**) Estimated copies per cell of PIM1 and PIM2 protein from published quantitative proteomics analysis (Howden et al., 2019; Brenes et al., 2023) of CD8 T cells expanded in IL-2 or IL-15 as outlined in Fig 2B. (B-D, F-G) WT (Ly5.1) and Pim dKO lymph node or spleen single cell suspensions were mixed at a 50:50 ratio of T cells, activated for 2 days with αCD3/αCD28 (both 0.5 µg/mL) and IL-2 (20 ng/mL), washed then split into fresh medium containing IL-2 (20 ng/mL) daily (as per Fig 2B). Some of the mixed cell suspensions were also cultured in IL-7 (5 ng/mL) to sustain a naïve T cell reference. (**B**) WT and Pim dKO CTL were treated 1 hour +/- Jak1/3 inhibitor Tofacitinib (100 nM) (negative control) before pSTAT5 Y694 expression was measured on day 3 and 6 of culture, (**C**) surface CD25 expression was measured on days 3 and 6 or culture, (**D**) CD8 T cell number vs time was calculated, (**F**) CD8 T cell FSC-A, SSC-A and surface activation markers (CD44, CD71) were measured on days 3 and 6 of culture (**G**) expression of adhesion molecule CD62L was measured daily. (**E**) WT and Pim dKO T cells were activated and expanded with IL-2 as per (Fig 3B-D, F-G) except in separate cultures and % live cells (PI-ve) was assessed on days 4 and 6 (two-way ANOVA).
Symbols in bar charts represent biological replicates, symbols in (D) represent the mean. Error bars show mean ± S.D. Data are representative of (B, G) n=4, (C,F) n=6 or show pooled data from (D) n=4, (E) n=6 biological replicates with data collected over at least 2 independent experiments

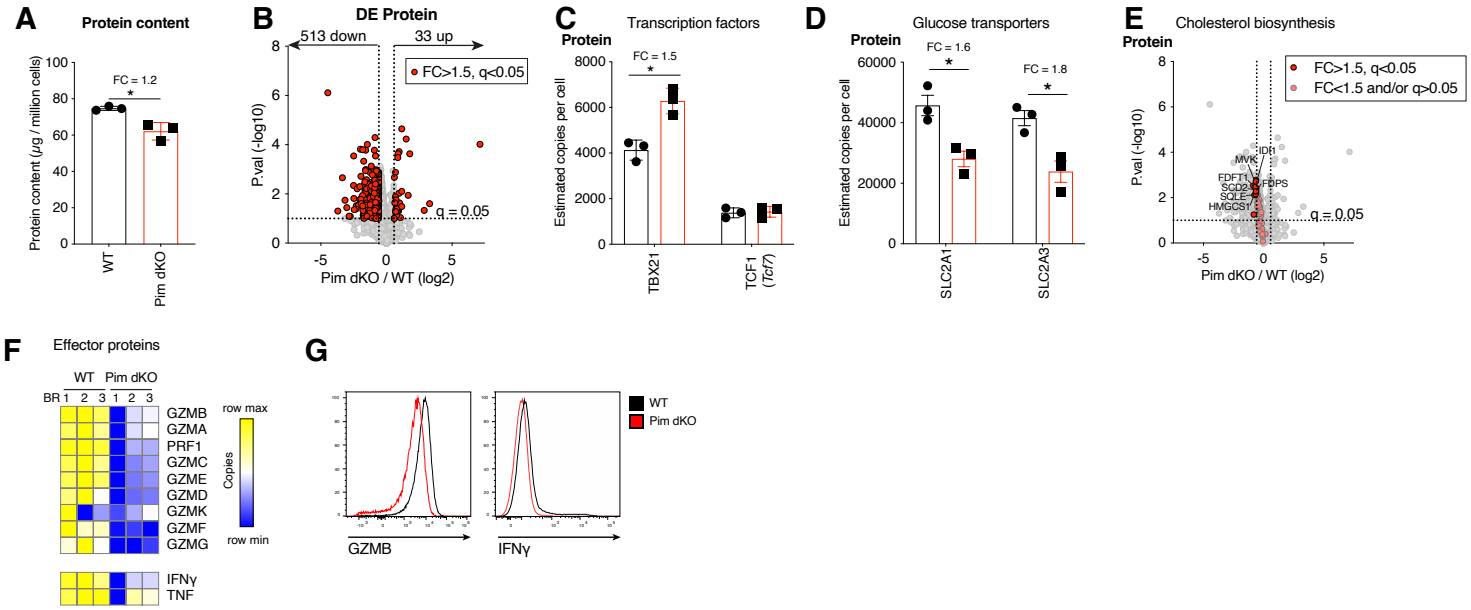

Figure 4. Major glucose transporters and effector proteins are reduced in Pim dKO IL-2 expanded CTL

WT and Pim dKO CD8 T cells were activated for 2 days with αCD3/αCD28 (both 0.5 µg/mL) and IL-2 (20 ng/mL), washed then split into fresh medium containing IL-2 (20 ng/mL) daily (as per Fig 2B), with an additional CD4 T cell magnetic depletion step on day 3 of culture. CD8 T cells were harvested on day 6 of culture for high resolution mass spectrometry. (**A**) Estimated total protein content per cell (student t-test). (**B**) Volcano plots Pim dKO vs WT protein copy numbers, differentially expressed proteins (FC>1.5, q<0.05) are highlighted in red. Estimated protein copy number per cell of (**C**) transcription factor TBX21 and TCF1 (**D**) glucose transporters SLC2A1 and SLC2A3. (**E**) Volcano plots Pim dKO vs WT protein copy numbers. Proteins with KEGG term = "terpenoid backbone biosynthesis", "biosynthesis of unsaturated fatty acids" or "steroid biosynthesis" are highlighted with proteins with FC>1.5, q<0.05 shown in red and proteins with FC<1.5 and/or q>0.05 shown in pink. (**F**) Heatmap of protein copy numbers for granzymes, perforin and effector cytokines. (**G**) Granzyme B and IFNγ expression was measured by flow cytometry in day 6 IL-2 expanded WT and Pim dKO CTL.

Symbols in bar charts show biological replicates. Error bars show mean ± S.D. Data are representative of (G) n = 3-4, with data collected over at least 2 independent experiment Quantitative proteomics was performed on biological triplicates. * indicates q<0.05, fold-change (FC) shown on graph when q<0.05

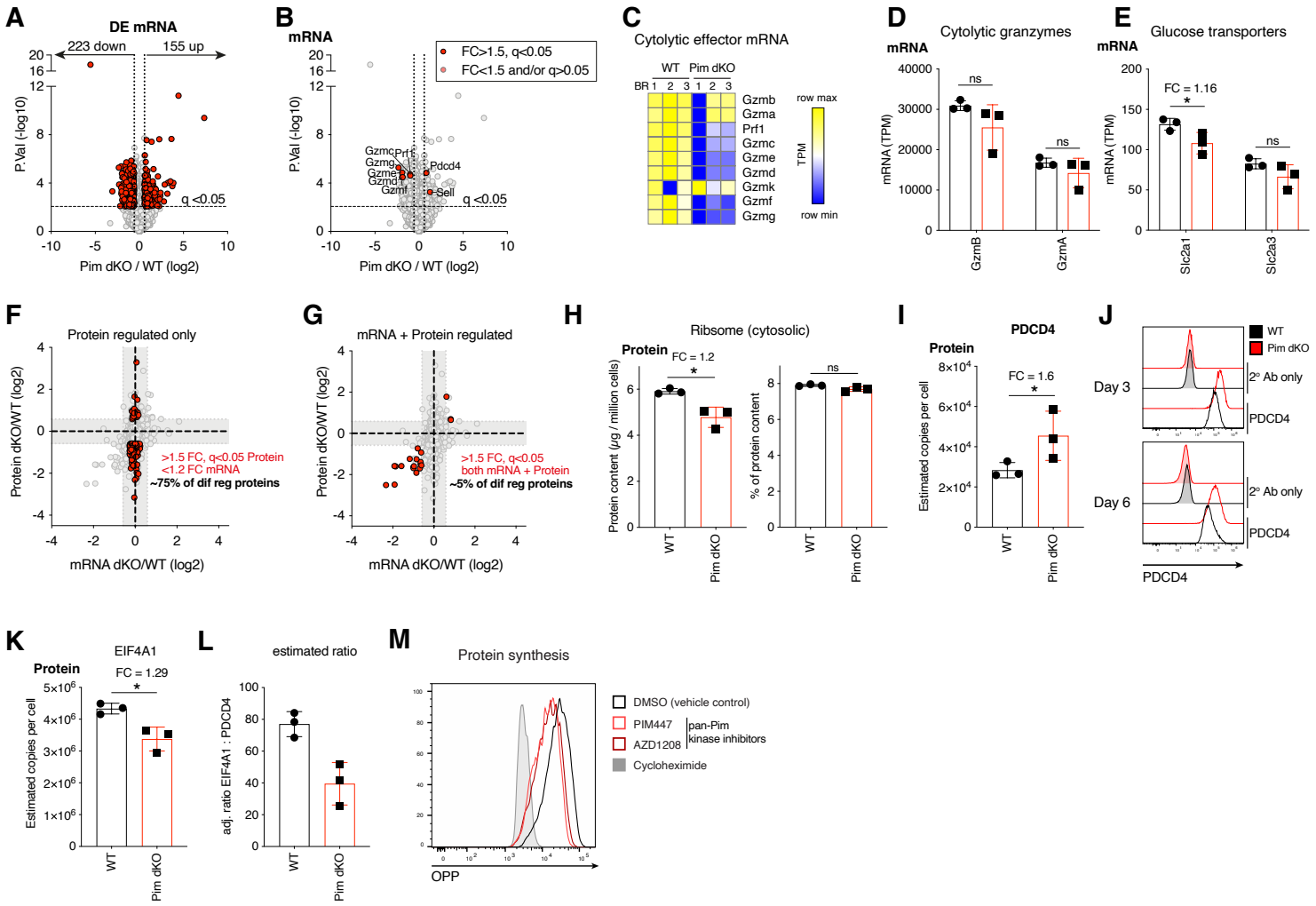

Figure 5. Disconnect between protein and mRNA expression in Pim1/Pim2-deficient effector CTL corresponds with a reduction in protein synthesis

RNAseq analysis was performed in day 6 IL-2 expanded WT and Pim dKO CD8 T cells which were collected in parallel with proteomics analysis described in Fig 4A. (**A**) Volcano plot of RNAseq data, differentially expressed mRNA (FC>1.5, q<0.05) are highlighted in red. (**B**) Volcano plot of RNAseq data, Granzymes C-K, perforin, Pdcd4 and Sell are highlighted in red. (**C**) Heatmap of mRNA expression (TPM) for granzymes, perforin and effector cytokines. Bar chart of mRNA expression (TPM) of (**D**) Granzymes A and B (**E**) Glucose transporters Slc2a1 and Slc2a3. (F-G) Fold change of PimdKO/WT protein (copies) from proteomics analysis described in Fig 4 vs mRNA (TPM) (**F**) highlighting in red proteins that are differentially expressed (FC>1.5, q<0.05) where mRNA is not substantially different (FC<1.2) and (**G**) highlighting in red protein and mRNA that are both differentially expressed (FC>1.5, q<0.05). (**H**) Estimated cytosolic ribosome content per cell (left), % ribosome of total cellular protein content (right). (**I**) Estimated protein copy number per cell of translation repressor PDCD4. (**J**) PDCD4 expression measured by flow cytometry on day 3 and 6 in IL-2 expanded WT vs Pim dKO CD8 T cells. (**K**) Estimated protein copy number per cell of EIF4A1. (**L**) adjusted ratio of PDCD4 : EIF4A1 (assuming 1 PDCD4 binds 2x EIF4A1) in WT and Pim dKO proteomes. (**M**) Protein synthesis measured by OPP incorporation in day 6 IL-2-expanded WT CTL treated for 24 hours with pan PIM kinase inhibitors PIM447 (5 µM) or AZD1208 (10 µM). 30 min cycloheximide (100 µg/mL) treatment gives no protein synthesis background control.

Symbols in bar charts show biological replicates: error bars show mean ± S.D. Data are representative of (M) n=2 biological replicates collected over two independent experiments, (J) n = 2 biological replicates. Quantitative proteomics and RNAseq were performed on biological triplicates. * indicates q<0.05, fold-change (FC) shown on graph when q<0.05.

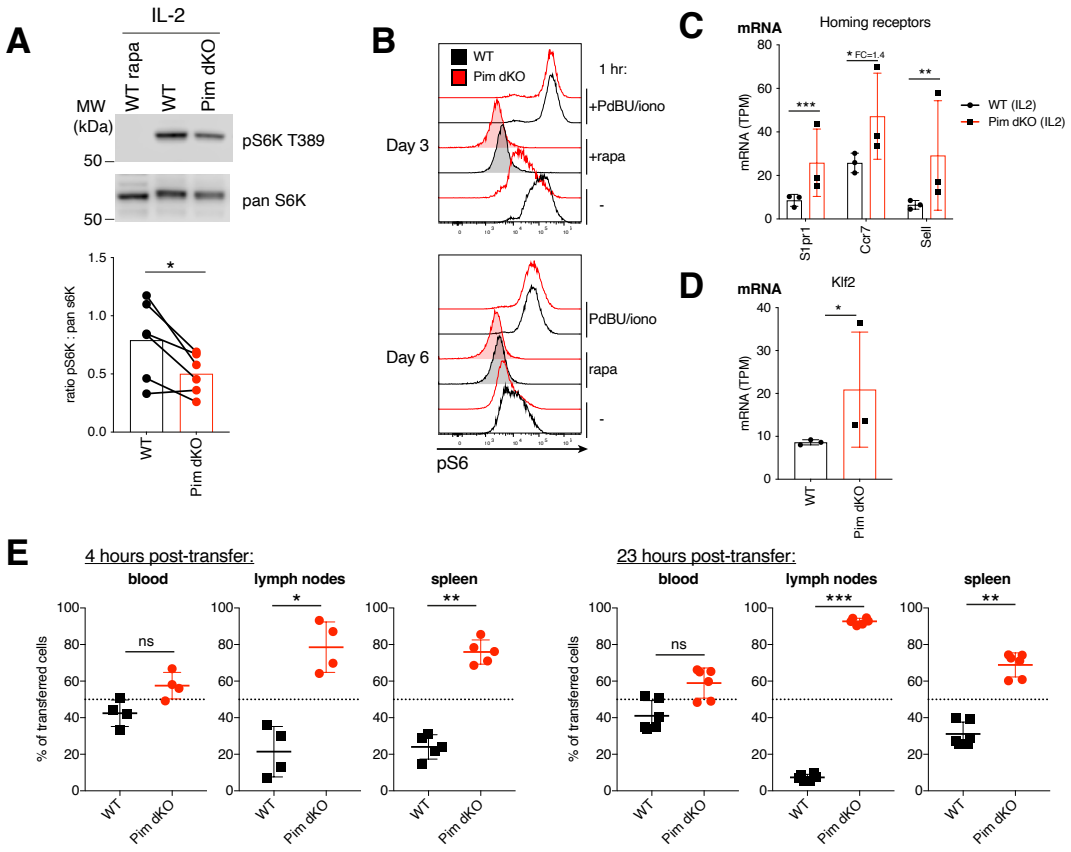

Figure 6. PIM kinases regulate mTORc1 activity and lymphoid homing in effector CTL

(**A**) Western blot of pS6K T389 and pan S6K from day 6 WT and PimdKO IL-2 CTL (paired student t-test, *= p<0.05). (**B**) WT and Pim dKO T cells were mixed in a 50:50 ratio, activated with αCD3/αCD28 (both 0.5 µg/mL) and IL-2 (20 ng/mL) and expanded in IL-2 as per Fig 2B and pS6 (Ser235/236) measured after 1 hr +/- PdBU and ionomycin (positive control), +/- rapamycin (mTORc1 inhibitor, negative control) or no additional treatment. mRNA expression (TPM) from RNAseq analysis of IL-2 expanded WT and Pim dKO CTL described in Fig 5A for (**C**) cell homing receptors S1pr1, Ccr7 and Sell and (**D**) transcription factor Klf2. (**E**) WT and Pim dKO T cells were activated and expanded with IL-2 in separate cultures as per Fig 2B. On day 6 of culture WT and Pim dKO CTL were labelled with CFSE or CTV, mixed at a 50:50 ratio and transferred into C57Bl/6 recipient mice. Values indicate percentage of transferred cells detected in blood, lymph node or spleen 4 or 23 hours post-transfer that were WT or Pim dKO (one-way ANOVA).

Symbols show biological replicates. Error bars show mean ± S.D. Data are representative of (A) n= 6, (B) n=2-4 collected across at least 2 independent experiments and (E) n= 6 recipient mice, from n=2 biological donor replicates. RNAseq was performed on biological triplicates. * q<0.05, ** q<0.01, *** q<0.001, fold-change (FC) shown on graph when q<0.05 but FC<1.5.

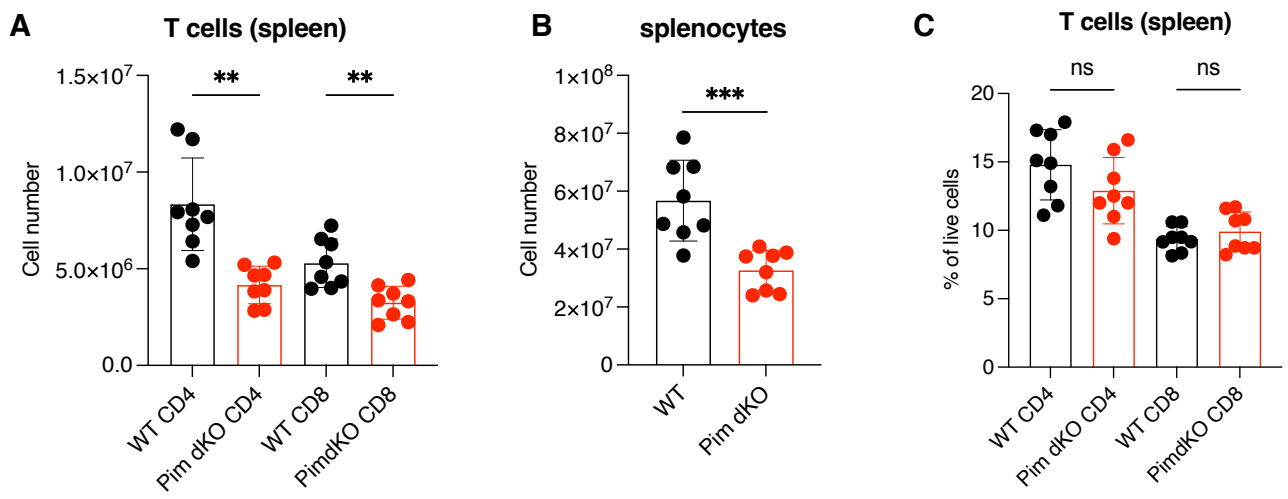

Figure S1. T cell counts in WT vs Pim dKO spleen

Comparison of Pim dKO and age/sex matched WT control mice for (**A**) total number of CD4 and CD8 T cells in spleens (one-way ANOVA), (**B**) total number of splenocytes (student t-test), (**C**) proportion of live splenocytes that were CD4 and CD8 (one-way ANOVA). Symbols in bar charts represent biological replicates: error bars show mean ± S.D. (A-C) n = 8 collected over 4 independent experiments. ** q<0.01, ***q<0.001.

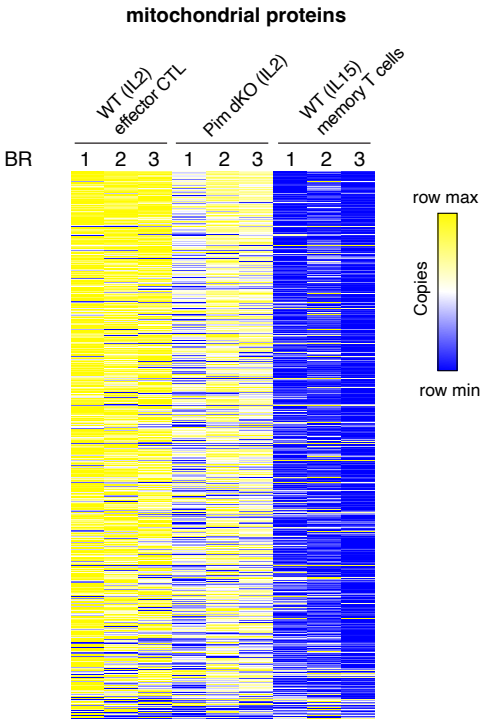

Figure S2. Pim dKO IL2 expanded CD8 T cells exhibit an effector-like mitochondrial proteome profile

Heatmap showing protein copy number of mitochondrial proteins (as defined by inclusion on Mitocarta 3.0 list) from IL-2 expanded WT (effector), Pim dKO and IL-15 expanded WT (memory) proteomics experiments described in Fig 2 and 4. Proteins are ranked based on average expression in IL2 WT condition. Proteomics was performed on biological triplicates.

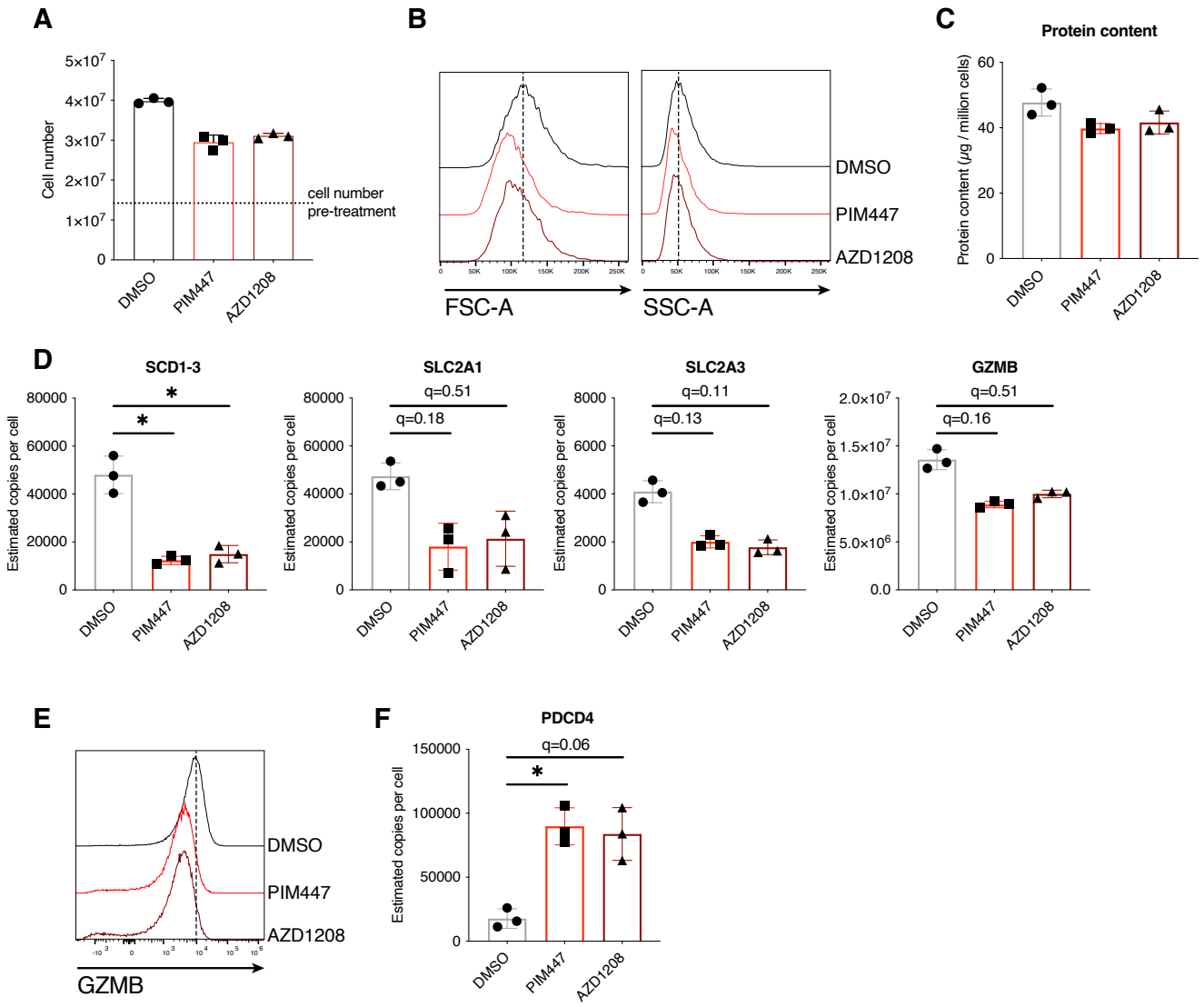

Figure S3. 24 hour treatment of IL-2 CTL with pan-PIM kinase inhibitors PIM447 or AZD1208 recapitulates many features of Pim1/Pim2-deficiency

Single cell suspension from P14 TCR-transgenic mouse lymph nodes were activated with gp33 peptide (100 ng/mL), IL-2 (20 ng/mL) and IL-12 (2 ng/mL) for 2 days, then split daily into fresh media containing IL-2 (20 ng/mL). On day 5 of culture IL-2 expanded CTL were treated with pan-PIM kinase inhibitors PIM447 (5 µM) or AZD1208 (10 µM) or DMSO vehicle control for 24 hours harvested on day 6 of culture to measure (**A**) Cell number (**B**) FSC-A SSC-A. Proteome analysis was also performed on inhibitor treated CTL to measure (**C**) protein content, (**D**) protein expression of SCD1-3, SLC2A1, SLC2A3, GZMB or (**F**) PDCD4. (**E**) Day 6 IL-2 expanded CTL from WT (C57BL/6) mice were treated for 24 hours with PIM447 or AZD1208 (both 1 µM) and GZMB expression was measured by flow cytometry.

Symbols show biological replicates. Error bars show mean ± S.D. Data are representative of (E) n=2 biological replicates collected across at least 2 independent experiments. Proteomics analysis was performed on biological triplicates, with (A-B) collected in parallel with proteomics analysis. * q<0.05.